NASA Technical Memorandum 80083

(NASA-TM-80083) INFLUENCE OF OPTIMIZED LEADING-EDGE DEFLECTION AND GEOMETRIC ANHEDRAL ON THE LOW-SPEED AERODYNAMIC CHARACTERISTICS OF A LOW-ASPECT-RATIO HIGHLY SWEPT ARROW-WING CONFIGURATION (NASA) 53 p HC A04/MF A01 G3/02

N79-27095

Unclas 29305

INFLUENCE OF OPTIMIZED LEADING-EDGE DEFLECTION AND GEOMETRIC ANHEDRAL ON THE LOW-SPEED AERODYNAMIC CHARACTERISTICS OF A LOW-ASPECT-RATIO HIGHLY SWEPT ARROW-WING CONFIGURATION

Paul L. Coe, Jr. and Jarrett K. Huffman

June 1979

National Aeronautics and Space Administration

Langley Research Center
Hampton, Virginia 23665

SUMMARY

An investigation has been conducted in the Langley 7- by 10-foot tunnel to determine the influence of an optimized leading-edge deflection on the low-speed aerodynamic performance of a configuration with a low-aspect-ratio, highly swept wing. Tests have also been conducted to determine the sensitivity of the lateral-stability derivative (C_{l_β}) to geometric anhedral.

The optimized leading-edge deflection was developed by aligning the leading edge with the incoming flow along the entire span. Owing to the spanwise variation of upwash, the resulting optimized leading edge was a smooth, continuously warped surface for which the deflection varied from 16° at the side of body to 50° at the wing tip. For the particular configuration studied, levels of leading-edge suction on the order of 90 percent were achieved with the smooth, continuously warped leading-edge contour. Attempts to approximate this smooth contour by a series of discrete deflections of a multi-segmented leading-edge system resulted in substantial increments in drag. The drag increments, introduced by the surface discontinuities of the multi-segmented system, markedly reduced the aerodynamic performance.

Deflecting the leading edge was found to provide a favorable reduction in the inherently high level of C_{l_β}. Comparison of experimental results with simple theoretical estimates of $\partial C_{l_\beta}/\partial C_L$ shows that excellent correlation exists for conditions of attached flow. Furthermore, the results of tests conducted to determine the sensitivity of C_{l_β} to geometric anhedral indicate values of $\partial C_{l_\beta}/\partial \Gamma$ which are in reasonable agreement with estimates provided by simple vortex-lattice theories.

INTRODUCTON

The National Aeronautics and Space Administration is currently investigating the aerodynamic characteristics of advanced aircraft concepts which are capable of cruising efficiently at supersonic speeds. These conceptual designs are representative of future generation commercial and military vehicles and incorporate wing sweeps on the order of 70° to 80°. (See, for example, refs. 1 and 2.) Unfortunately, owing to the high wing sweeps, such configurations have traditionally exhibited unacceptable low-speed characteristics. The most significant of these unacceptable characteristics being deficiencies in low-speed performance and excessively high levels of effective dihedral (C_{l_β}). The present investigation is part of the Swept-Wing Aerodynamic Technology (SWAT) effort. This effort is intended to yield fundamental information necessary to provide highly swept-wing designs with acceptable low-speed characteristics.

Previous low-speed studies with a configuration having the same wing geometry as the present model are reported in references 3 to 6. The present study was specifically intended to: (1) provide an assessment of the aerodynamic performance benefits which could be achieved with a suitably optimized leading edge; and (2) determine the sensitivity of the lateral-stability derivative (C_{l_β}) to geometric anhedral.

The tests were conducted in the Langley 7- by 10-foot tunnel over an angle-of-attack range from about -6° to 15° for sideslip angles of 0° and ±5°. The tests were conducted at a Reynolds number (based on the wing mean aerodynamic chord) of about 2.8×10^6.

SYMBOLS

The longitudinal data are referred to the stability system of axes, and the lateral-directional data are referred to the body system of axes as illustrated in figure 1. The moment reference center for the tests was located at 59.166 percent of the wing-reference mean aerodynamic chord. The wing-reference area and reference mean aerodynamic chord are based on the wing planform which results from extending the inboard (74°) leading-edge sweep angle and the outboard (41.457°) trailing-edge sweep angle to the model center line. (See fig. 2.)

The dimensional quantities herein are given in both the International System of Units (SI) and the U.S. Customary Units.

A_{fus}	fuselage cross-sectional area, m^2 (ft^2)
AR	aspect ratio
b	wing span, m (ft)
C_D	drag coefficient, Drag/qS_{ref}
C_{D_i}	induced drag coefficient
$C_{D_{min}}$	minimum drag coefficient
$C_{D_{sym}}$	drag coefficient of equivalent configuration without twist and camber at zero lift
C_L	lift coefficient, Lift/qS_{ref}
C	rolling-moment coefficient, Rolling moment/$qS_{ref}b$
C_m	pitching-moment coefficient, Pitching moment/$qS_{ref}\bar{c}$
C_n	yawing-moment coefficient, Yawing moment/$qS_{ref}b$
C_Y	side-force coefficient, Side force/qS_{ref}
$\bar{c}$	reference mean aerodynamic chord, m (ft)

q	free-stream dynamic pressure, Pa (lbf/ft^2)
S	leading-edge suction parameter
S_{ref}	reference wing area, m^2 (ft^2)
X,Y,Z	body axis coordinates
X_{fus}	fuselage body station, origin at nose, positive rearward, m (ft)
α	angle of attack, deg
β	angle of sideslip, deg
Γ	increment in geometric anhedral, relative to the basic wing geometry, at span station y, deg
Γ_1, Γ_2	increment in geometric anhedral, relative to the basic wing geometry, at span stations y_1 and y_2, respectively, deg (see fig. 2(a))
$\delta_{L.E.}$	leading-edge deflection, positive when leading edge is down, deg
ϵ	upwash angle, deg
ξ	X-Y projection of the included angle between the local flow direction at the leading edge and a ray normal to the leading-edge hinge line, deg (see fig. 1)

Derivatives:

$C_{L_\alpha} = \partial C_L/\partial\alpha$, per degree

$C_{l_\beta} = \partial C_l/\partial\beta$, per degree

$C_{n_\beta} = \partial C_n/\partial\beta$, per degree

$C_{Y_\beta} = \partial C_Y/\partial\beta$, per degree

MODEL

The dimensional characteristics of the model used in the present study are listed in table 1 and shown in figures 2 and 3. The wing geometry is in conformance with the cruise shape geometry defined in reference 7. A photograph of the model in the Langley 7- by 10-foot tunnel is presented in figure 4.

Previous studies with configurations having the same wing geometry as the present model are reported in references 3 through 6. The present study was intended to address generic problems associated with highly swept wings;

consequently, the model did not incorporate either nacelles or an aft fuselage. The model did, however, incorporate a multi-segmented leading edge which permitted continuously variable deflections from 0° to 60° about the 70.688° swept hinge line. (See fig. 2.) This particular hinge line was selected to allow a direct comparison with results from reference 5. The model further incorporated anhedral breaks at span stations $y/_{b/2}$ = 0.234 and 0.736 which permitted the inclusion of additional geometric anhedral.

TESTS AND CORRECTIONS

The investigation was conducted in the Langley 7- by 10-foot high-speed tunnel. (See ref. 8 for a description of the tunnel.) Forces and moments were measured with a standard six-component strain-gage balance mounted internal to the model. The tests were conducted at a dynamic pressure of 1436.4 Pa (30 lbf/ft^2). This value of dynamic pressure resulted in a Reynolds number (based on the wing mean aerodynamic chord) of 2.8 x 10^6 at a corresponding Mach number of 0.14. The angle of attack ranged from about -6° to 15° for sideslip angles of 0° and ±5°. Both angle of attack and sideslip have been corrected for the effect of sting and balance bending under aerodynamic load.

The data have been corrected for jet-boundary and blockage effects using the methods outlined in reference 9 and 10, respectively. Balance chamber pressure and model base pressure were measured and the drag measurements adjusted to correspond to conditions of free-stream static pressure acting over the base of the model.

In accordance with the method of reference 11, 0.16 cm (0.0625 in.) wide transition strips of no. 70 carborundum grains were placed 3.81 cm (1.5 in.) aft of the leading edges of the wing and outboard vertical tails. Similarly, no. 80 carborundum grains were placed 3.81 cm (1.5 in.) aft of the model nose.

PRESENTATION OF RESULTS

A run schedule and tabular listing of data are provided in the data supplement at the end of this report. The results and discussion are presented in accordance with the following outline:

RESULTS AND DISCUSSION

The present study was intended to address generic problems associated with highly swept wings; therefore, the model did not incorporate either nacelles or an aft fuselage. In order to provide some insight into the possible effects such configuration components may have on absolute quantities, suitable comparisons are made (where possible) with data obtained for a model which had the same wing geometry, but included both underwing nacelles and an aft fuselage (see ref. 5). It should be noted, however, that in addition to the obvious nacelle and aft fuselage differences, the model of reference 5 incorporated a fuselage with a different cross-sectional area distribution (see fig. 3). In as much as the fuselages of both the present model and the model of reference 5 had the same centroidal axis, the difference in cross-sectional area also results in a difference in wing-body intersection.

Longitudinal Aerodynamic Characteristics

Configuration with undeflected leading edge.- Figure 5 presents the longitudinal aerodynamic characteristics for the present configuration with undeflected leading edges ($\delta_{L.E.} = 0$). At low angles of attack ($\alpha < 2^{\circ}$), the lift and pitching-moment coefficients are seen to be fairly linear. The lift-curve slope and neutral point are evaluated to be 0.037 deg^{-1} and 0.5505 $\bar{c}$, respectively and are in reasonable agreement with the theoretically predicted values (0.036 and 0.5312 $\bar{c}$) discussed in reference 6. For angles of attack from about 2° to 4°, the flow over the main wing panels remains well attached; however, previous studies (see ref. 5), using smoke-flow visualization have indicated the existence of a tightly wound vortex formed close to the surface along the leading edge of the outboard wing panel. As might be anticipated, the existence of this tightly wound vortex is found to be accompanied by a small increase in longitudinal stability. At angles of attack greater than $\alpha = 4^{\circ}$, the data indicate the existence of a vortex-lift increment and a corresponding pitch-up tendency. This result is attributed to the simultaneous formation of classical wing-apex vortices and to the separation of the tightly wound vortex from the outboard wing panel.

Figure 6 presents a comparison of the data of figure 5 with the corresponding data from reference 5. The data of reference 5 exhibit trends which are identical to those of the present model. However, the geometric differences result in differences in the quantative values. Obviously, the lower value of drag exhibited by the present model results from the reduced skin-friction and interference drag associated with the omission of the aft fuselage and underwing nacelles. The negative increment in the pitching moment of the present model is attributed to the omission of the down-loaded aft fuselage (see ref. 5). The difference in the vortex-lift increment for the two configurations is not well understood. However, this difference probably arises from the difference in the wing-body intersection which may affect the formation of the wing-apex vortices.

Effect of leading-edge deflection.- Figure 7 presents the longitudinal aerodynamic characteristics for the configuration with a uniform 30° deflection of the entire leading edge (see fig. 2). As has been shown in reference 5, this leading-edge deflection results in fairly well attached flow for angles of attack from about 0° to 8°. For angles of attack greater than 8°, flow-visualization studies show the onset of a classical leading-edge vortex separation originating at about the mid-point of the wing semispan. It should also be noted, that at very low angles of attack ($\alpha < 0°$), deflecting the leading edges, apparently results in flow separation on the lower wing surfaces as evidenced by the nonlinearity in C_L versus α. Figure 7 also presents the longitudinal aerodynamic data from reference 5 for the comparable ($\delta_{L.E.} = 30°$) condition. As can be seen, the differences in data for the present tests and reference 5 are generally similar to those previously discussed for the $\delta_{L.E.} = 0°$ condition. As expected, with the leading edges deflected to suppress the leading-edge vortices, excellent agreement in C_L versus α is obtained over the angle-of-attack range tested.

Figure 8 provides a comparison of the data for the conditions of $\delta_{L.E.} = 0°$ and 30°. As has been noted in reference 5, deflecting the wing leading edges to eliminate the vortex flow reduces the undesirable vortex induced pitch-up tendency and also reduces the vortex related drag. In order to permit a quantative evaluation of the performance improvement achieved by leading-edge deflection, figure 8 also presents the theoretical polars corresponding to the conditions of: (1) minimum induced drag (100-percent leading-edge suction) and (2) full leading-edge separation with no subsequent flow attachment (0-percent leading-edge suction). These conditions are defined herein as

$$C_D = C_{D_{sym}} + C_L^2/\pi AR \tag{1}$$

and

$$C_D = C_{D_{sym}} + C_L \tan (C_L/C_{L_\alpha}) \tag{2}$$

It should be noted that equations (1) and (2) are, of course, valid only for symmetric wings with no twist or camber and are presented herein solely to permit the aerodynamic performance (achieved by the various leading-edge treatments) to be quantified. This is accomplished by introducing the leading-edge suction parameter S (see ref. 12 for a comprehensive discussion of leading-edge suction) defined herein as

$$S = \frac{C_D - [C_{D_{sym}} + C_L \tan (C_L/C_{L_\alpha})]}{C_L^2/ AR - C_L \tan (C_L/C_{L_\alpha})} \tag{3}$$

It should be noted than in equations (2) and (3), the quantity $C_L \tan (C_L/C_{L_\alpha})$ has been used in place of the more customary $C_L \tan\alpha$. (See ref. 12.) This present notation has been introduced to insure a common basis for comparison of leading-edge suction for the various leading-edge treatments. The value of $C_{D_{sym}}$ has been estimated for the present model tests using the relationship

$$C_{D_{sym}} = C_{D_{min}} + \frac{C_L^2 \big|_{@C_{D_{min}}}}{AR} \qquad (4)$$

ORIGINAL PAGE IS OF POOR QUALITY

Evaluation of equation (4) yields $C_{D_{sym}} = 0.0096$. The value of C_{L_α} has been determined experimentally (for the linear region of C_L versus α) to be 0.037 and, as mentioned previously, is in agreement with theoretical results.

Figure 9 presents the calculated values of leading-edge suction. As can be seen, the uniform 30° deflection results in substantially increased values relative to the $\delta_{L.E.} = 0°$ condition. This result is similar to the results presented in reference 5, wherein this uniform 30° deflection was intially considered. As pointed out in reference 5, the uniform 30° does not represent an optimum condition. In fact, the uniform 30° deflection is considered to be over-deflected in the apex region, while being under-deflected further outboard. This situation developed because the leading-edge system tested in reference 5 was limited to four segments, and attempts to optimize the leading-edge deflection by aligning the leading edge with the local upwash (as will be discussed) resulted in large discontinuities in contour. These large discontinuities were found to result in quite pronounced regions of separated flow, which substantially degraded the performance. Consequently, the uniform 30° deflection was considered an appropriate compromise.

In as much as the present configuration employed a multi-segmented leading edge (which could be capable of approximating a continuously warped surface), an attempt was made to optimize the spanwise variation of leading-edge deflection. The optimal leading edge is considered herein as one for which the leading edge is aligned with the upwash along the entire span. Since $\alpha = 10°$ is representative of the angle-of-attack condition for low-speed operations, attempts were made to obtain attached flow for angles of attack at least up to this condition.

Figure 10 presents the theoretical spanwise variation of upwash (ϵ) obtained with a vortex-lattice computational model at an angle of attack of 10° (see refs. 5 and 13). In general, for a swept hinge line, the angular deflection required to align the leading edge with an upwash angle ϵ would be defined by the standard relationship of sweep theory

$$\delta_{L.E.} = \tan^{-1}\left[\frac{\tan\epsilon}{\cos\xi}\right] \qquad (5)$$

However, previous smoke flow-visualization studies (see ref. 5) have shown that the incoming flow is approximately perpendicular to the hinge line ($\xi = 0°$), and therefore, equation (5) yields the simple result that $\delta_{L.E.} = \epsilon$.

With the model at $\alpha = 10°$ and with the leading edge deflected to approximate the upwash schedule of figure 10, observtions of wool surface tufts revealed flow separation originating outboard of $y/_{b/2} = 0.5$. This result appeared to be attributal to the fairly sharp corner introduced by rather high deflection about the simple hinge line. Accordingly, the leading-edge deflection of the inboard span was reduced until a condition was reached wherein further reductions resulted in classical leading-edge vortex separation. The multi-segmented leading edge was then faired and smoothed to eliminate leading-edge discontinuities. The spanwise variation of leading-edge deflection, as developed above, is compared in figure 11 with the theoretical upwash. The leading-edge deflection schedule is seen to define a continuously warped surface which varies from 16° inboard to 50° outboard. This leading-edge geometry will herein after be designated as $\delta_{L.E.} = 16^\circ - 50^\circ$.

Figure 12 presents the longitudinal aerodynamic characteristics obtained with $\delta_{L.E.} = 16^\circ - 50^\circ$, while figure 13 presents a comparison of these data with the previously discussed results for the $\delta_{L.E.} = 0^\circ$ and 30° conditions. As can be seen, the data for $\delta_{L.E.} = 16^\circ - 50^\circ$ indicate attached flow conditions for angles of atack from about 0° to 10°. At angles of attack above 10°, vortex separation was observed to originate along the leading edge outboard of $y/_{b/2}$ = 0.5. The occurence of this leading-edge separation is seen to be consistent with the slight pitch-up characteristic exhibited by the data of figure 12.

The leading-edge suction parameter obtained with the above continuously warped leading-edge geometry ($\delta_{L.E.} = 16^\circ - 50^\circ$) is presented in figure 14. As can been seen, $\delta_{L.E.} = 16^\circ$ results in a substantial improvement in the aerodynamic performance relative to the previous $\delta_{L.E.} = 30^\circ$ geometry. In particular, $\delta_{L.E.} = 16^\circ - 50^\circ$ is seen to achieve values of suction on the order of 90 percent at representative second segment climb conditions (i.e., $C_L \approx 0.3$). However, at higher values of C_L the level of leading-edge suction is substantially reduced. It should be noted that the model tested did not employ trailing-edge flaps, and therefore, the higher values of C_L were achieved at fairly high angles of attack. Consequently, the values of S presented for the high-lift conditions are not representative. Based on the results presented in reference 5, it is anticipated that the use of a trailing-edge flap system would permit increased levels of suction to be achieved for the high-lift condition.

The effect of Reynolds number on the leading-edge suction parameter has been discussed in reference 12. The results presented therein indicate that increasing the Reynolds number from the low values of the present tests to actual flight values will result in only modest increases in S for the separated flow condition (e.g., the condition discussed herein with $\delta_{L.E.} = 0^\circ$). However, for attached flow conditions (as achieved with $\delta_{L.E.} = 16^\circ - 50^\circ$), increasing Reynolds number results in pronounced increases in S. Based on these results, it would appear that the level of leading-edge suction parameter achieved with the attached flow, $\delta_{L.E.} = 16^\circ - 50^\circ$ deflection is conservative.

It is recognized that while the continuously warped leading edge would provide marked improvements in low-speed aerodynamic performance, the mechanical complexity required to generate this smooth contour from the high-speed cruise shape may limit its practical application. Correspondingly, tests were conducted in which the leading-edge deflection ($\delta_{L.E.} = 16^\circ - 50^\circ$) was preserved, but the fairing between the adjacent segments of the multi-segmented system removed. Figure 15 presents a comparison of the longitudinal data obtained with $\delta_{L.E.} = 16^\circ - 50^\circ$ for both faired and unfaired conditions. As can be seen, the impact of removing the leading-edge fairings is largely limited to an increase in drag. This result correlates well with observations made of wool tufts

ORIGINAL PAGE IS
OF POOR QUALITY

during the limited flow visualization portion of the tests. Although no large regions of separation could be attributed to the removal of the segment fairings, the tufts were observed to be slightly more unsteady, thereby indicating localized regions of separation. Consideration of the leading-edge suction parameter presented in figure 16 shows that the discrete multi-segmented leading edge with $\delta_{L.E.} = 16^{o} - 50^{o}$ exhibits levels of the leading-edge suction parameter which are below those values achieved with the simple uniform 30^{o} deflection.

Lateral-Directional Characteristics

Configuration with undeflected leading edge.- Figure 17 presents the lateral-directional stability derivatives for the present configuration with undeflected leading edges. Also presented in figure 17 are corresponding results from reference 5 which, as previously mentioned, were obtained with a model which had the same wing geometry but incorporated a different fuselage and included under-wing nacelles. As can be seen from figure 17, both configurations exhibit neutrally stable values of static directional stability (C_{n_β}) for angles of attack up to about 4^{o}. For angles of attack greater than 4^{o} (corresponding to the angle of attack for which the wing-apex-vortices are first evident), the configuration exhibits a marked increase in C_{n_β}. This phenomenon has been observed previously (see ref. 5) and has been attributed to the interaction of the wing-apex vortices with the forward portion of the configuration.

The data of figure 17 also show that both configurations exhibit high levels of effective dihedral (C_{l_β}), as would be expected for the low-aspect-ratio wing. References 14 and 15 have shown that these high levels of C_{l_β} typically result in Dutch roll instabilities and reversals in pilot-commanded roll rates. The analysis of reference 4 has also shown that, because of limited lateral-control capabilities (typical of low-aspect-ratio wings), the high values of C_{l_β} would necessitate excessive approach speeds to meet currently accepted cross-wind landing requirements.

It is interesting to note that although both the present configuration and the configuration of reference 5 exhibit about the same slope of C_{l_β} versus α, the magnitude of C_{l_β} for the present configuration is reduced. This reduction in C_{l_β} is believed to be due to the omission of the under-wing nacelles and to a difference in the aft wing-body intersection.

Effect of wing leading-edge deflection.- Figure 18 presents the lateral-directional stability derivatives for the configuration with $\delta_{L.E.} = 0^{o}, 30^{o}$, and $16^{o} - 50^{o}$. As can be seen by comparison of the results presented, both of the deflected leading edge geometries resulted in a reduction in C_{n_β}. The reduction in C_{n_β} at low angles of attack is simply due to the deflected leading edge providing an increased vertical area forward of the moment reference center. At higher angles of attack, the dramatic reduction in C_{n_β} is, of course, associated with the suppression of the wing-apex-vortices. Although this reduction in C_{n_β} at high angles of attack may appear to be adverse, previous studies (see ref. 17) have shown that positive increments in

C_{n_β}, when originating forward of the center of gravity (as is the case considered herein), are accompanied by undesirable reductions in damping in yaw. Consequently, deflection of the leading edge may also improve the high angle-of-attack directional stability characteristics.

The data of figure 18 also indicate that deflecting the leading edge yields a favorable increment in C_{l_β}. This result is primarily due to the simple increase in geometric anhedral which accompanies the leading-edge deflections. Figure 19 presents these same data as the variation of C_{l_β} with respect to C_L for the various leading-edge deflections. Noted on the figures are the regions of separated and attached flow, as discussed in connection with figures 5, 7, and 12. As can be seen by comparison of the results presented for the conditions under which attached flow exists, positive increments in C_{l_β} of 0.00016 and 0.00022 are obtained (relative to $\delta_{L.E.} = 0^o$) for $\delta_{L.E.} = 30^o$ and $16^o - 50^o$, respectively.

It should be noted, that for conditions of attached flow, $\partial C_{l_\beta}/\partial C_L$ is found to be independent of leading-edge geometry and has a value of -0.0058. This value of $C_{l_\beta}/\partial C_L$ is in excellent agreement with the value of -0.0061 obtained from the expression

$$\partial C_{l_\beta}/\partial C_L = \frac{2}{3} \cdot \frac{1}{AR} \cdot \frac{2\pi}{360} \qquad (6)$$

which is developed in reference 18. The break in the slope of C_{l_β} versus C_L is a product of flow separation. In as much as a properly designed configuration would be intended to operate with attached flow, the values of C_{l_β} for conditions of separated flow are not applicable. Extrapolation of the attached flow results to higher lift coefficients (as could be achieved with a simple trailing-edge flap system) shows that the configuration would exhibit values of C_{l_β} of about -0.003 at a nominal approach lift coefficient of 0.6.

Effect of geometric anhedral.- The results of the preceding section indicates that, as expected, high values of C_{l_β} are inherent to the low-aspect-ratio highly swept wing. Consequently, tests were conducted in order to determine the sensitivity of C_{l_β} to additional geometric anhedral and to correlate these results with existing theory. These tests were conducted with the geometric anhedral increased at span stations $y/_{b/2}$ = 0.234 and 0.736 (see fig. 1). The leading-edge geometry for the configuration during this phase of the study was limited to the continuously warped $\delta_{L.E.} = 16^o - 50^o$ condition, which was previously found to exhibit superior longitudinal performance. Examination of the tabulated data (presented in the data supplement at the end of this report) for the various anhedral angles tested shows that the longitudinal variables were not influenced by anhedral. The data further show that the geometric anhedral does not have any significant effect on the directional stability characteristics. Consequently, the discussion is limited to a consideration of the influence of geometric anhedral on C_{l_β}.

ORIGINAL PAGE IS
OF POOR QUALITY

Figure 20 presents the variation of $C_{l\beta}$ with C_L for the various anhedral angle combinations tested. From theoretical considerations, it would be expected that the values of $\partial C_{l\beta}/\partial \Gamma$ (as determined by cross-plotting the data of fig. 20) would be constant for attached flow conditions. However, analysis of the data of figure 20 shows that $\partial C_{l\beta}/\partial \Gamma$ increases with increasing lift coefficient. To determine the additive nature of the experimental results for $C_{l\beta}$ versus C_L, a selected combination of $\Gamma_1 = 4^o$ and $\Gamma_2 = 11^o$ was tested. The experimental results (see fig. 21) are seen to compare well with results obtained by adding the experimentally determined incremental values of $C_{l\beta}$ presented in figure 20.

Figure 22 presents the theoretical variation of $\partial C_{l\beta}/\partial \Gamma$ as a function of the corresponding nondimensional semispan location. The theoretical results were obtained with a vortex-lattice computational model which is based on the theory of reference 13. The range of experimental results for $\partial C_{l\beta}/\partial \Gamma$, evaluated from figure 20 at $C_L = 0.2$ and 0.4, are presented for comparison. It is noted that although the experimental values of $\partial C_{l\beta}/\partial \Gamma$ have been shown to increase with increasing C_L, they are in reasonable agreement with the theoretical results. Furthermore, both the vortex-lattice theoretical results and the experimental results are seen to be in agreement with the approximate values of $\partial C_{l\beta}/\partial \Gamma$ obtained using the simple design chart procedure contained in reference 19.

The results presented in figure 22 indicate that quite substantial reductions in $C_{l\beta}$ may be achieved by introducing geometric anhedral at inboard span locations. However, it should be recognied that a detailed configuration study is required to determine the most effective means of incorporating such additional anhedral.

As an illustration, the simplified analysis presented in the appendix considers the case wherein anhedral is added at an inboard span location. The analysis assumes that the wing-tip clearance remains unchanged as would be required for the case where the landing gear length was held constant. Obviously, under these conditions, adding geometric anhedral at inboard locations necessitates the addition of dihedral at outboard locations. The results presented in the appendix show that for these conditions, the net resulting improvement in $C_{l\beta}$ is negligible.

SUMMARY OF RESULTS

The results of a study to determine the influence of optimized leading-edge deflection and geometric anhedral on the low-speed performance and lateral stability of configurations with highly swept wings may be summarized as follows:

1. Leading-edge deflection is effective in suppressing the formation of wing-apex-vortices and promoting attached flow conditions.

2. Due to the spanwise variation of upwash, the optimal leading edge deflection is a smooth, continuously warped surface. For the particular configuration

ration studied, levels of leading-edge suction on the order of 90-percent are achieved with a smooth, continuously varying leading-edge deflection corresponding to 16° at the side-of-body and increasing to 50° at the wing tip.

3. Small discontinuities in surface contour, introduced in an attempt to approximate the smooth continuously warped leading edge with a series of discrete deflections of a multi-segmented leading-edge system, resulted in large increments in drag and corresponding large reductions in the leading-edge suction parameter.

4. A uniform leading-edge deflection of 30° (representing an average value of the continuously warped leading-edge deflection) provided higher values of the leading-edge suction parameter than provided by the discrete multi-segmented system. This result is apparently due to the elimination of the small surface discontinuities introduced by deflecting the individual segments through different angles.

5. Deflecting the entire leading edge to achieved attached flow is found to provide a favorable reduction in the inherently high level of C_{l_β} which is associated with the low-aspect-ratio highly swept wing.

6. The theoretical value of $\partial C_{l_\beta}/\partial C_L$ is found to be in excellent agreement with experimental results for conditions where attached flow exists.

7. The inclusion of additional geometric anhedral to reduce the high levels of C_{l_β} is found to yield values of $\partial C_{l_\beta}/\partial \Gamma$ which are in reasonable agreement with theoretical estimates.

APPENDIX

Effect of Geometric Anhedral on C_{l_β}

The following simple analysis is intended to illustrate the effect on C_{l_β} of increasing the geometric anhedral of the configuration reported herein. The analysis assumes that the wing-tip clearance remains unchanged, as would be required for the case wherein the landing gear length is held constant.

Consider the wing semispan sketched in figure A-1. The spanwise location of the anhedral breaks, and the corresponding anhedral angles define the change in vertical height of the wing tip as

$$Z_{TIP} = \Gamma_i \,(b/2 - y_i) + \Gamma_o \,(b/2 - y_o) \qquad \text{(A-1)}$$

where the subscripts i and o refer to the values associated with assumed inboard and outboard locations, respectively. Requiring $Z_{TIP} = 0$ and solving for Γ_o yields

$$\Gamma_o = -\Gamma_i \,\frac{1 - \dfrac{y_i}{b/2}}{1 - \dfrac{y_o}{b/2}} \qquad \text{(A-2)}$$

As shown in the body of this report (see figs. 20 and 21), the increment in C_{l_β} resulting from Γ_i and Γ_o may be determined by linear combination; therefore

$$\Delta C_{l_\beta} = \frac{\partial C_{l_\beta}}{\partial \Gamma_i} \cdot \Gamma_i + \frac{\partial C_{l_\beta}}{\partial \Gamma_o} \cdot \Gamma_o \qquad \text{(A-3)}$$

Substituting equation (A-2) into equation (A-3) yields

$$\Delta C_{l_\beta} = \left[\frac{\partial C_{l_\beta}}{\partial \Gamma_i} - \left(\frac{1 - \dfrac{y_i}{b/2}}{1 - \dfrac{y_o}{b/2}} \right) \cdot \frac{\partial C_{l_\beta}}{\partial \Gamma_o} \right] \Gamma_i \qquad \text{(A-4)}$$

Evaluation of equation (A-4) shows that, for the variation of $\partial C_{l_\beta}/\partial \Gamma$ presented in figure 22, maintaining constant wing-tip clearance would limit the favorable increments in C_{l_β} to negligible values. For example, consider the result for

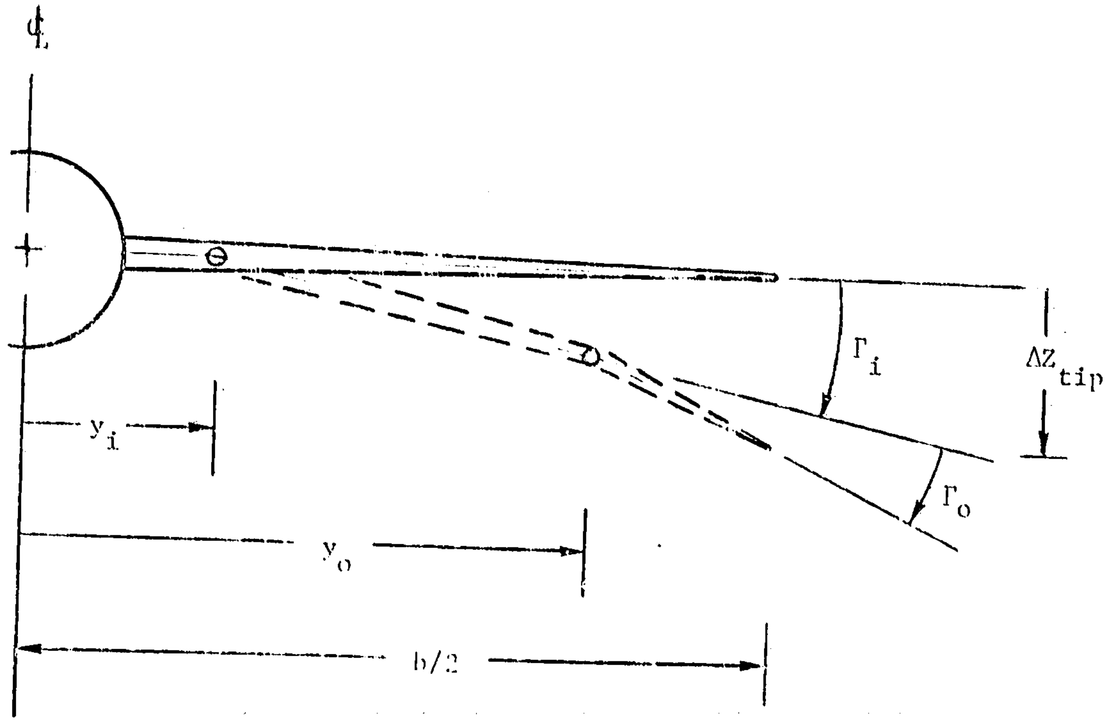

$$\Delta Z_{tip} = \Gamma_i \left(\frac{b}{2} - y_i\right) + \Gamma_o \left(\frac{b}{2} - y_o\right)$$

for $\Delta Z_{tip} = 0$

$$\Gamma_o = -\Gamma_i \frac{1 - y_i/\frac{b}{2}}{1 - y_o/\frac{b}{2}}$$

Figure A.- Geometric relationship of anhedral angles and wingtip height.

the spanwise location of anhedral breaks tested on the present configuration. At span locations $y_i/b/2 = 0.234$ and 0.736, the theoretical results of figure 22 show $\partial C_{l_\beta}/\partial \Gamma_i = 0.85 \times 10^{-4}$ and $\partial C_{l_\beta}/\partial \Gamma_o = 0.27 \times 10^{-4}$. Assuming the anhedral at the inboard location is increased by 5° (with no constraint on wing-tip clearance); the increment in C_{l_β} for this condition would be $\Delta C_{l_\beta} = 4.25 \times 10^{-4}$. However, constraining the change in wing-tip clearance to zero, reduces the increment to $\Delta C_{l_\beta} = 0.33 \times 10^{-4}$.

REFERENCES

1. Robins, A. Warner; Morris, Odell A.; and Harris, Roy V., Jr.: Recent Results in the Aeodynamics of Supersonic Vehicles. J. Aircraft, vol. 3, 1966, pp. 573-577

2. Robins, A. Warner; Lamb, Milton; and Miller, David S.: Aerodynamic Characteristics at Mach Numbers of 1.5, 1.8, and 2.0 of a Blended Wing-Body Configuration With and Without an Integral Canard. NASA TP 1427, 1979

3. Coe, Paul L., Jr.; McLemore, H. Clyde; and Shivers, James P.: Effects of Upper Surface Blowing and Thrust Vectoring on Low-Speed Aerodynamic Characteristics of a Large-Scale Supersonic Transport Model. NASA TN D-8296, 1976

4. Coe, Paul L., Jr.; Smith, Paul M.; and Parlett, Lysle P.: Low-Speed Wind-Tunnel Investigation of an Advanced Supersonic Cruise Arrow-Wing Configuration. NASA TM 74043, 1977

5. Coe, Paul L., Jr.; and Weston, Robert P.: Effects of Wing Leading-Edge Deflection on the Low-Speed Aerodynamic Characteristics of a Low-Aspect-Ratio Highly Swept Arrow-Wing Configuration. NASA TM 78787, 1978

6. Coe, Paul L., Jr.; and Thomas, James L.: Theoretical and Experimental Investigation of Ground Induced Effects for a Low-Aspect-Ratio Highly Swept Arrow-Wing Configuration. NASA TM 80041, 1979

7. Staff, Hampton Technical Center, LTV Aerospace Corporation: Advanced Supersonic Technology Concept Study Reference Characteristics. NASA CR 132374, 1973

8. Fox, Charles H., Jr.; and Huffman, Jarrett K.: Calibration and Test Capabilities of the Langley 7- by 10-Foot High-Speed Tunnel. NASA TM X-74027, 1977

9. Gillis, Clarence L.; Polhamus, Edward C.; and Gray, Joseph L., Jr.: Charts for Determining Jet Boundary Corrections for Complete Models in 7 x 10 Foot Closed Rectangular Wind Tunnels. NACA ARR L5G31, 1945

10. Pope, A.; and Harper, J. J.: Low-Speed Wind-Tunnel Testing, John Wiley & Sons, Inc., New York, N.Y., 1966

11. Braslow, Albert L.; and Knox, Eugene C.: Simplified Method for Determination of Critical Height of Distribution Roughness Particles for Boundary-Layer Transition at Mach Number From 0 to 5. NACA TN 4363, 1958

12. Henderson, William P.: Studies of Various Factors Affecting Drag Due to Lift at Subsonic Speeds. NASA TN D-3584, 1966

13. Tulinius, J.: Unified Subsonic, Transonic, and Supersonic NAR Vortex Lattice. Rep. TFD-72-253, Rockwell International Corporation, 1972

14. Grantham, William D.; Nguyen, Luat T.; Deal, Perry L.; Neubauer, M. J., Jr.; Smith, Paul M.; and Gregory, Frederick D.: Ground Based and In-Flight Simulator Studies of Low-Speed Handling Characteristics of Two Supersonic Cruise Transport Concepts. NASA TP 1240, 1978

15. Coe, Paul L., Jr.; and Gilbert, William P.: Application of Low-Speed Aerodynamic Characteristics of Highly Swept Arrow-Wing Configuration to Supersonic Cruise Tactical Fighters Designs. AFFDL-TR-77-85, Air Force Flight Dynamics Laboratory, vol. I, July 1972

16. Etkin, Bernard: Dynamics of Flight Stability and Control. John Wiley & Sons, New York, N.Y., 1959

17. Grafton, Sue B.; Chambers, Joseph R.; and Coe, Paul L., Jr.: Wind-Tunnel Free-Flight Investigation of a Model of a Spin Resistant Fighter Configuration. NASA TN D-7716, 1974

18. Ribner, Herbert S.: The Stability Derivatives of Low-Aspect-Ratio Triangular Wings at Subsonic and Supersonic Speeds. NACA TN 1423, 1947

19. Campbell, John P.; and McKinney, Marion O.: Summary of Methods for Calculating Dynamic Lateral Stability and Reponse and for Estimating Lateral Stability Derivatives. NACA TN 2409, 1951

Table

Dimensional Characteristics of Model

Wing:	
Reference area, m² (ft²)	0.834 (8.972)
Gross area, m² (ft²)	0.919 (9.889)
Span, m (ft)	1.260 (4.133)
Root chord, m (ft)	1.674 (5.492)
Tip chord, m (ft)	0.161 (0.529)
Reference mean aerodynamic chord, m (ft)	0.880 (2.887)
Gross mean aerodynamic chord, m (ft)	1.038 (3.406)
Leading-edge sweep, deg	
At body station 0.388 m (1.272 ft)	74.0
At body station 1.427 m (4.683 ft)	70.5
At body station 1.886 m (6.185 ft)	60.0
Vertical fin (two):	
Area, m² (ft²)	0.041 (0.437)
Span, m (ft)	0.107 (0.350)
Root chord, m (ft)	0.326 (1.069)
Tip chord, m (ft)	0.048 (0.158)
Leading-edge sweep, deg	73.4

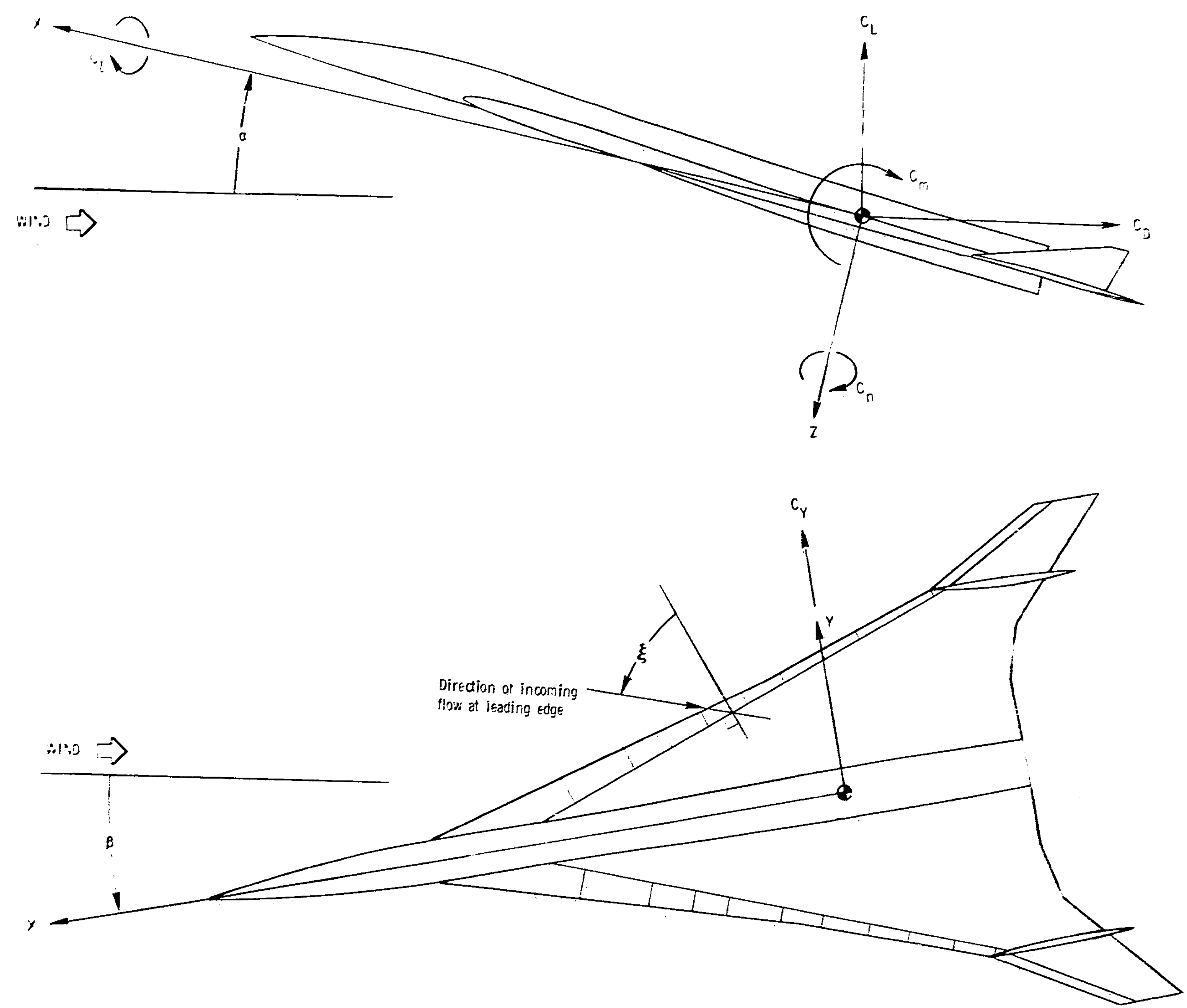

Figure 1. - System of axes and angular notation.

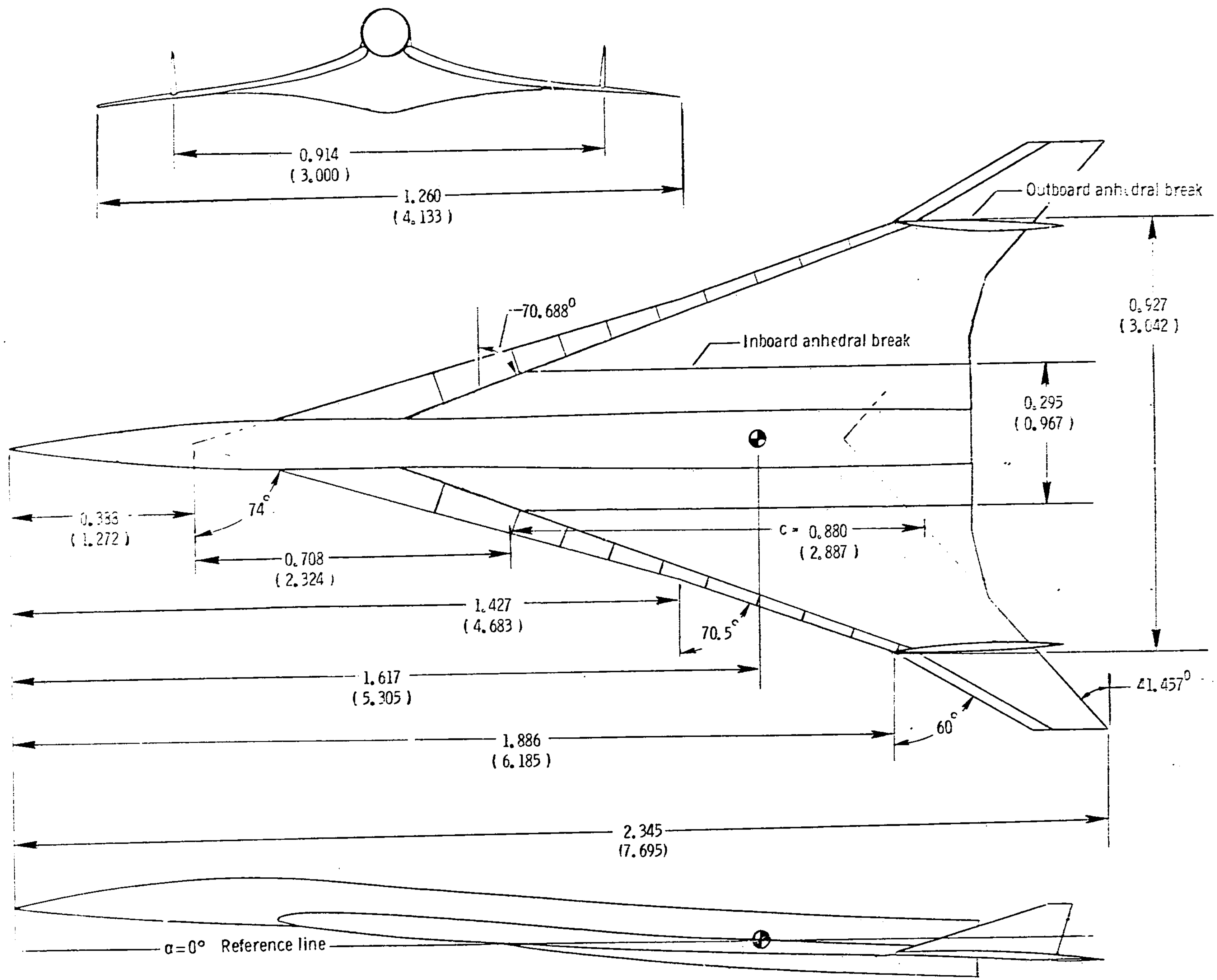

(a) Three-view sketch of model

Figure 2.- Geometric characteristics. Dimensions are given in meters and parenthetically in feet.

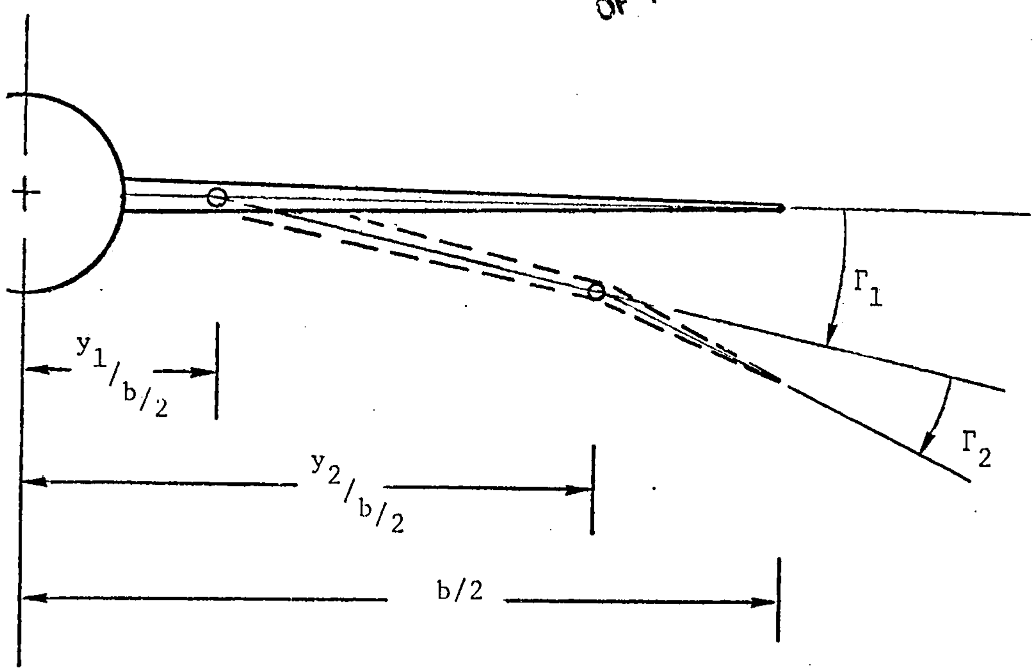

(b) Sketch showing anhedral angles

Figure 2.- Concluded.

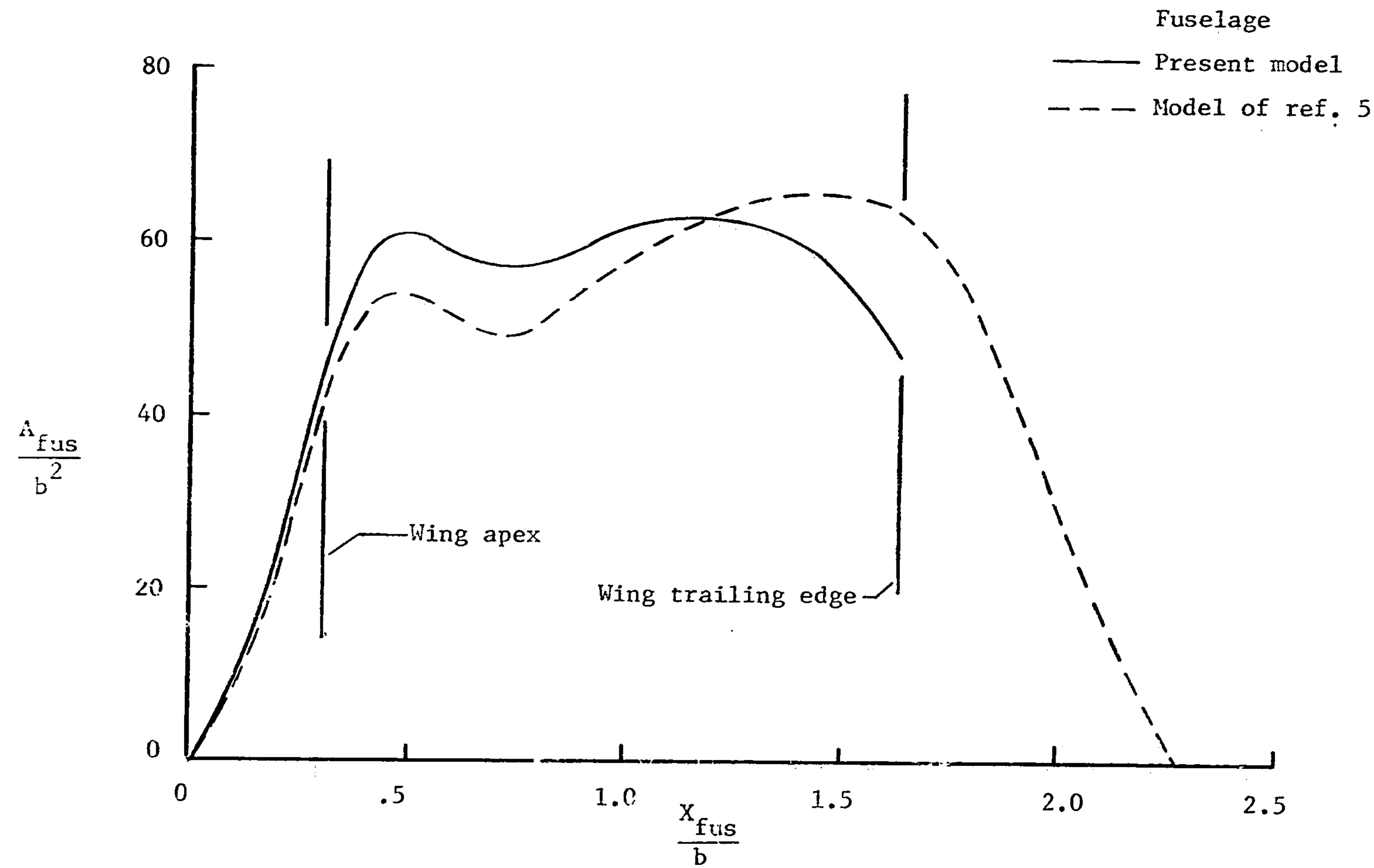

Figure 3.- Comparison of fuselage cross-sectional areas of present model and model of reference 5.

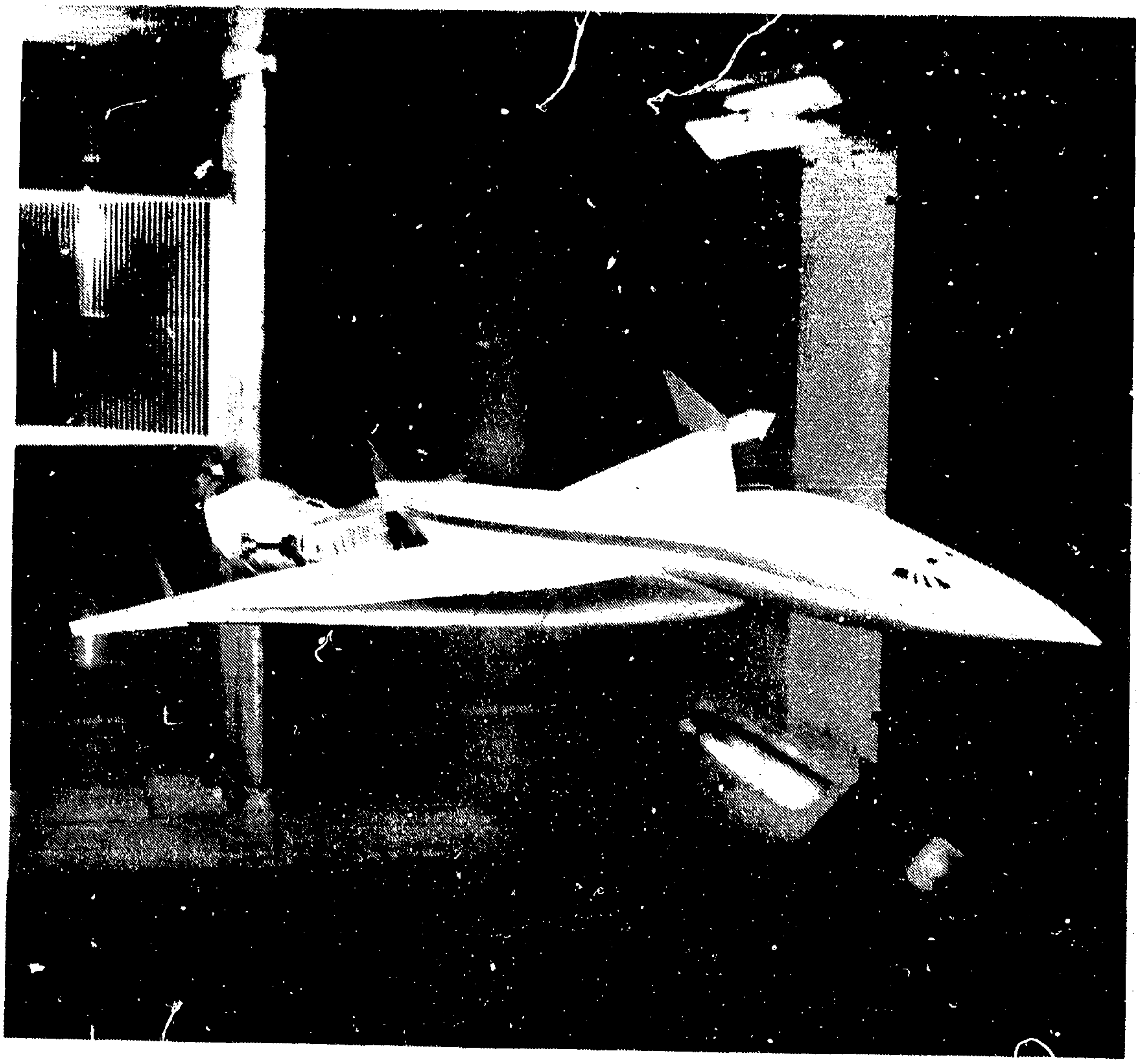

Figure 4.- Photograph of model in Langley 7- by 10-foot high-speed tunnel.

ORIGINAL PAGE IS
OF POOR QUALITY

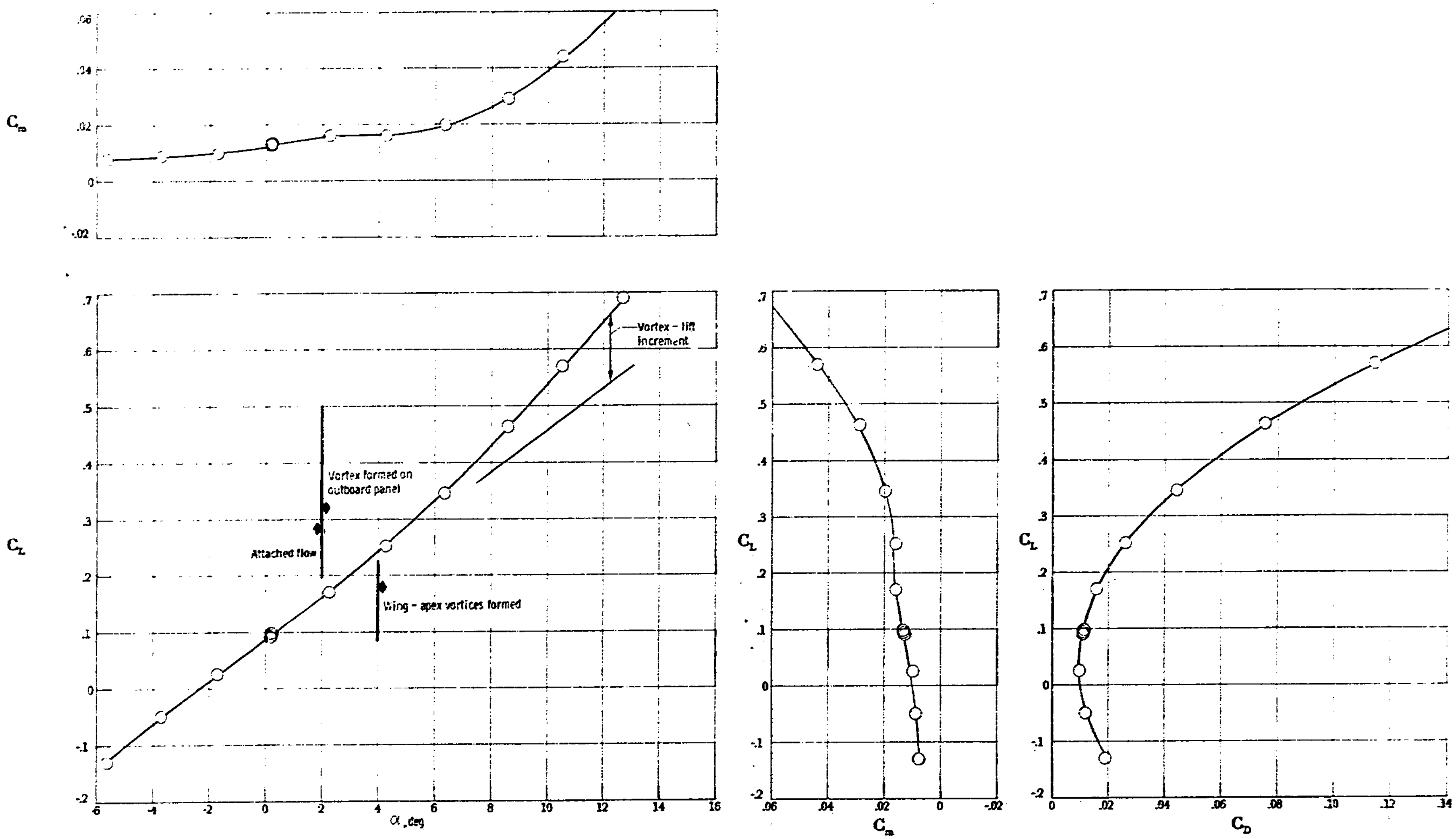

Figure 5.- Longitudinal aerodynamic characteristics of the configuration with $\delta_{L.E.} = 0^0$.

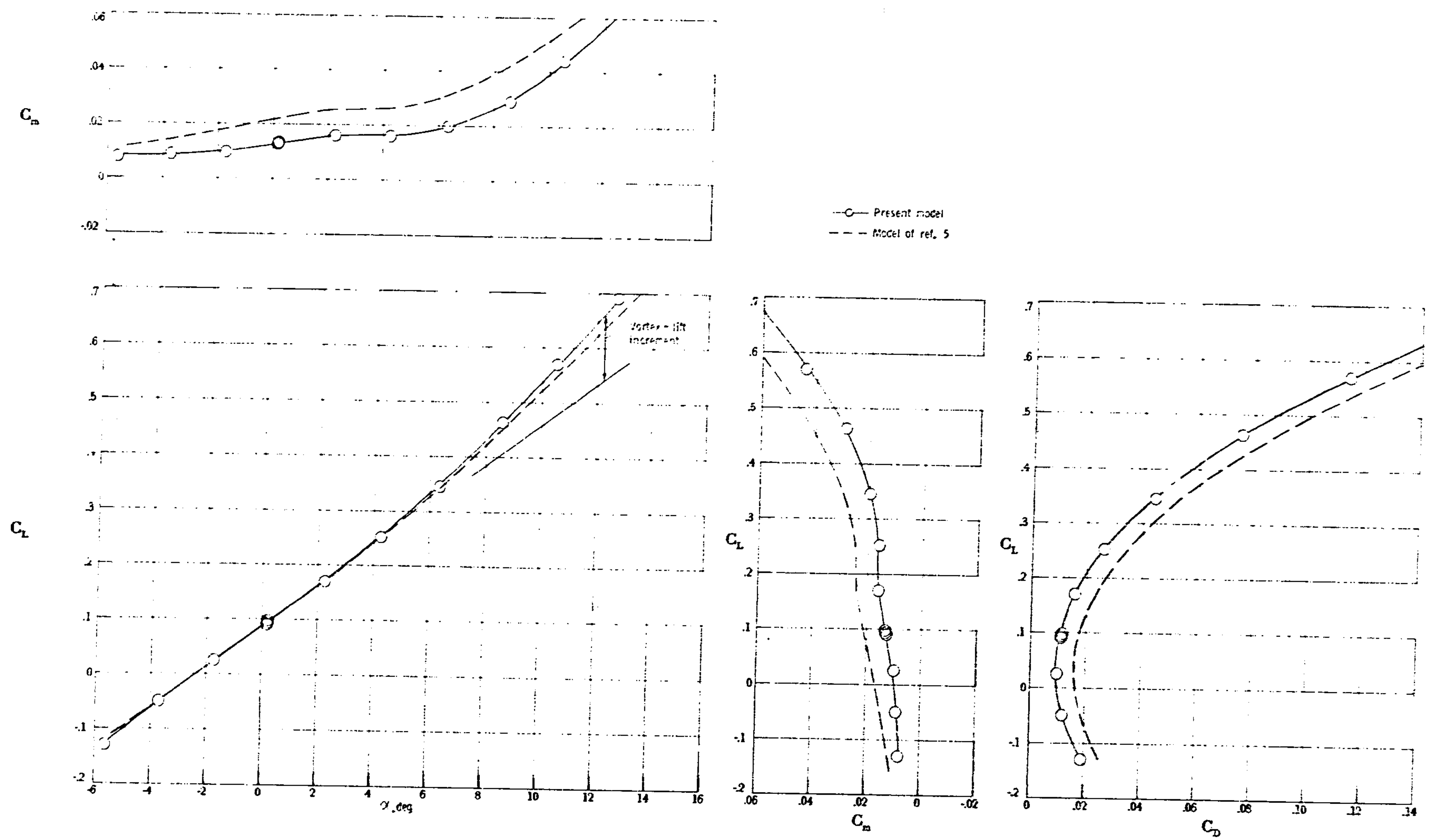

Figure 6.- Comparison of longitudinal aerodynamic data from present tests, with data determined for related configuration of reference 5. $\delta_{L.E.} = 0^{\circ}$.

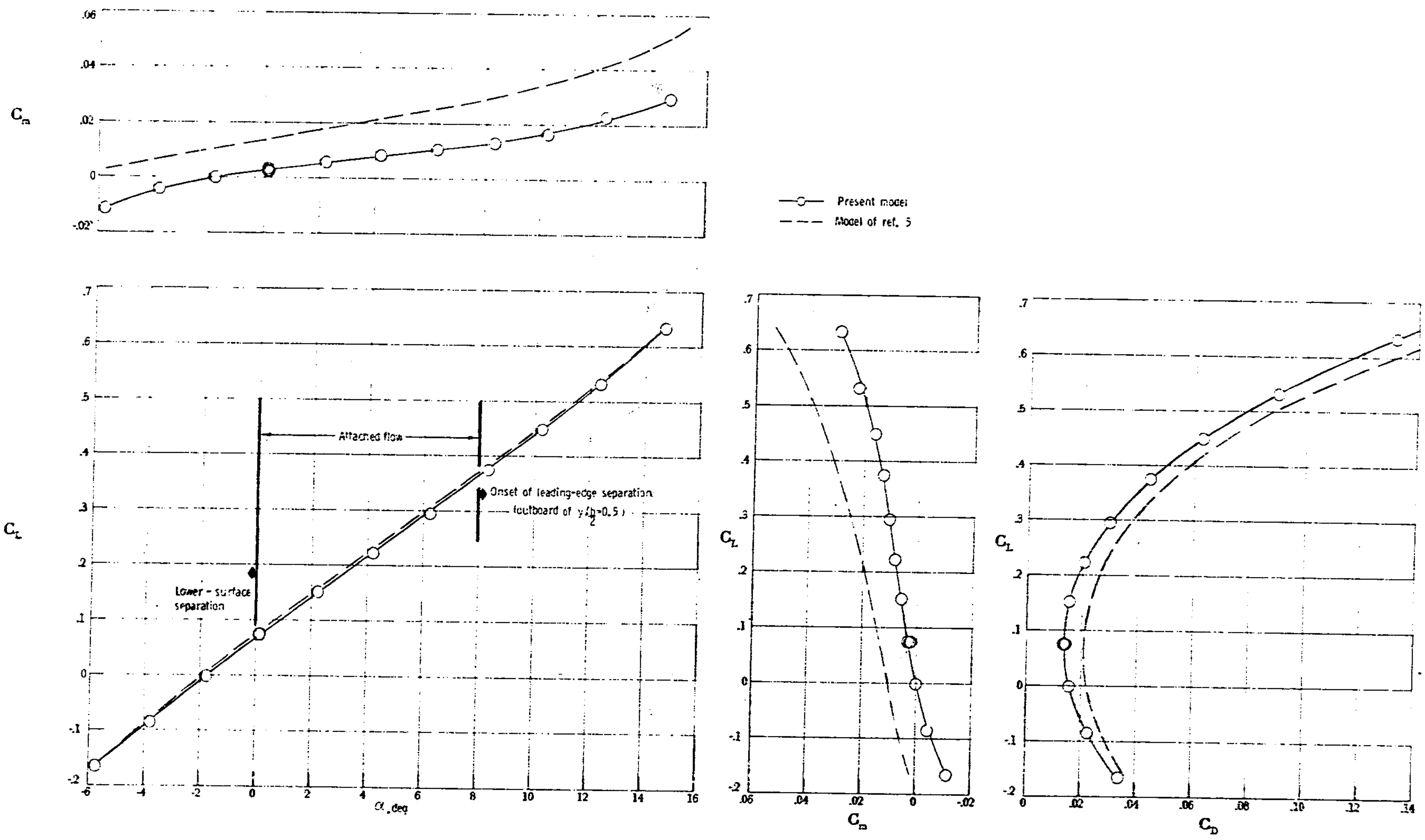

Figure 7.- Comparison of longitudinal aerodynamic data from present tests, with data determined for related configuration of reference 5. $\delta_{L.E.} = 30^{\circ}$.

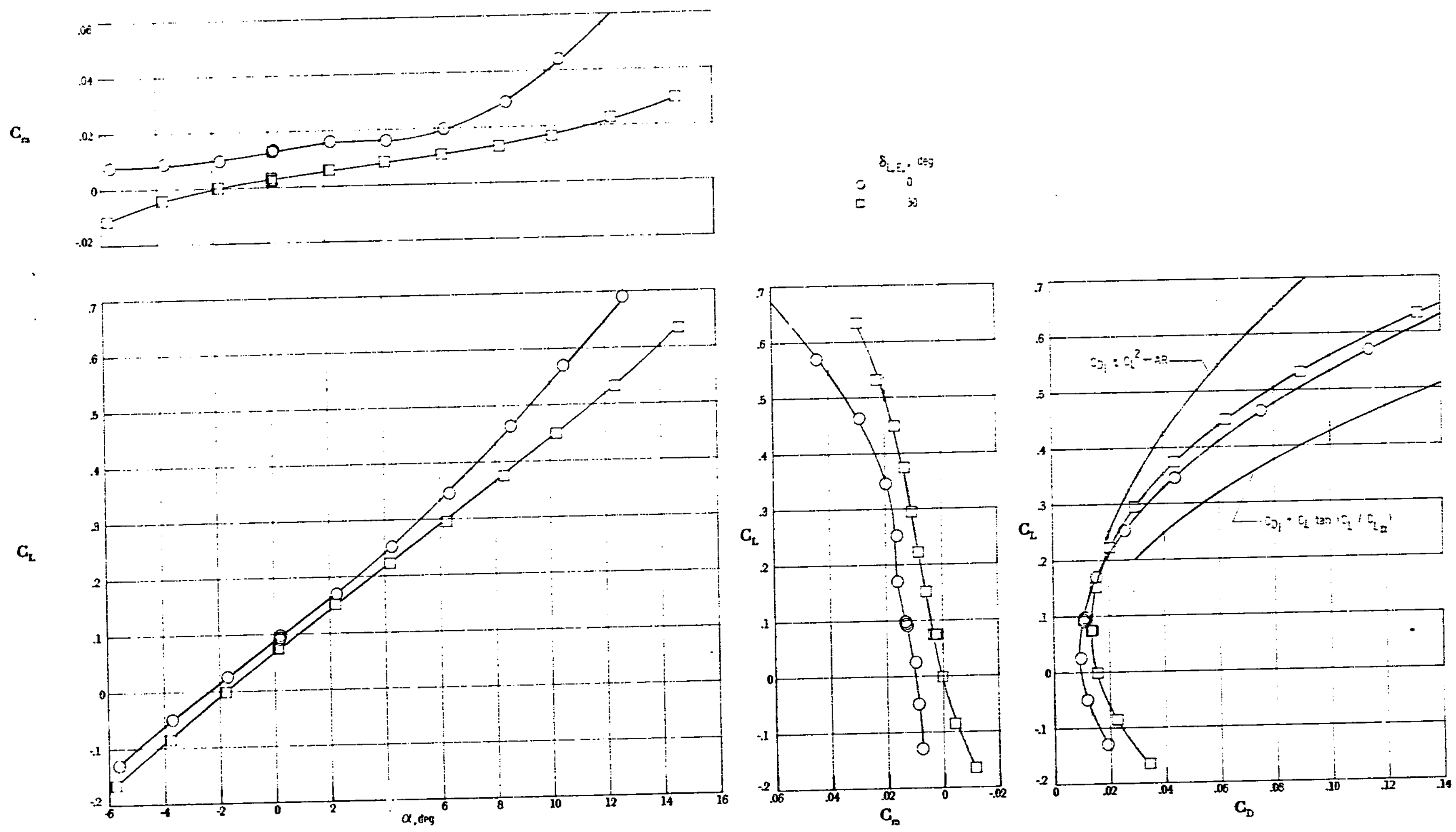

Figure 8.- Effect of wing leading-edge deflection on longitudinal aerodynamic characteristics.

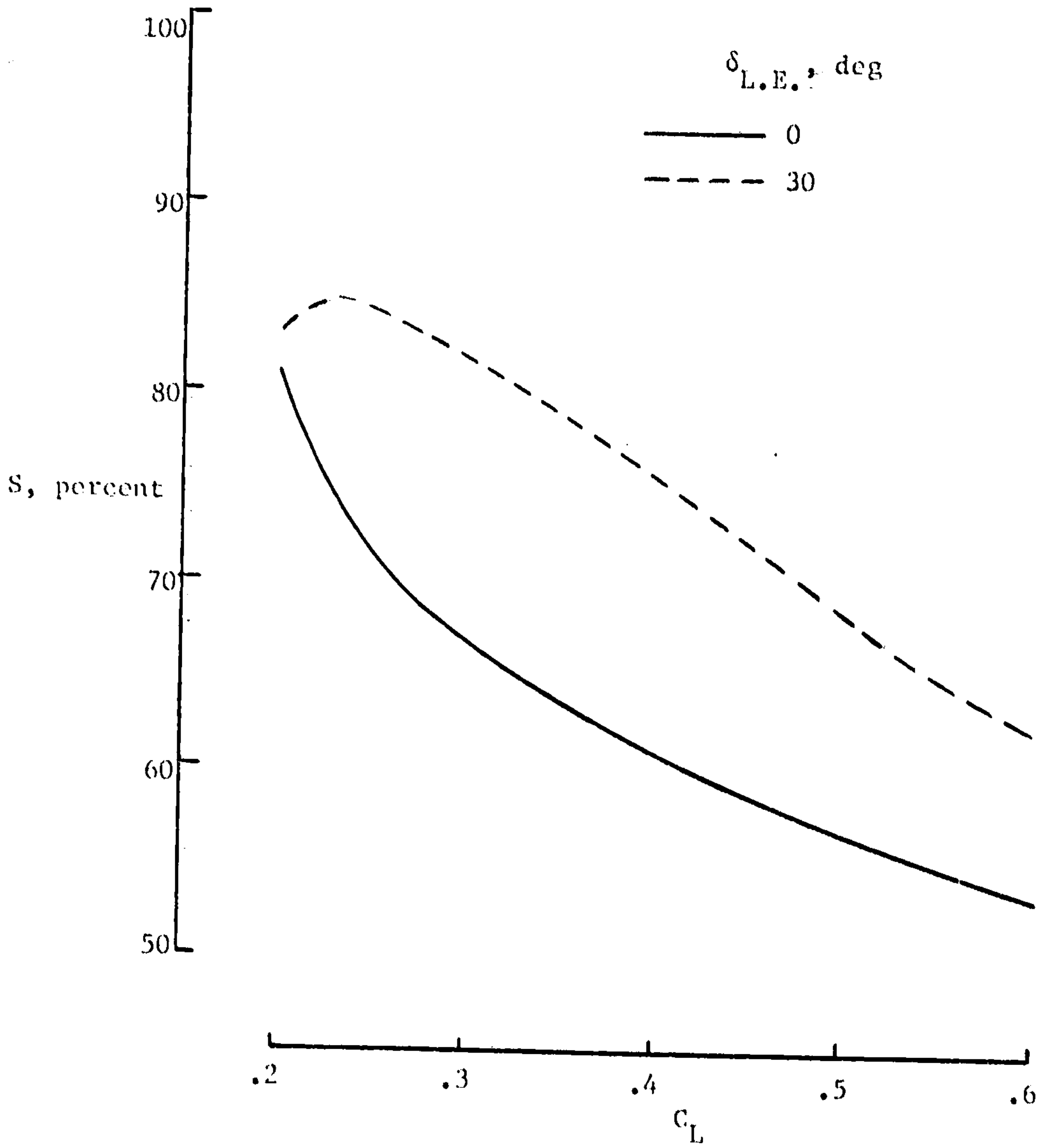

Figure 9.- Effect of leading-edge deflection on leading-edge suction.

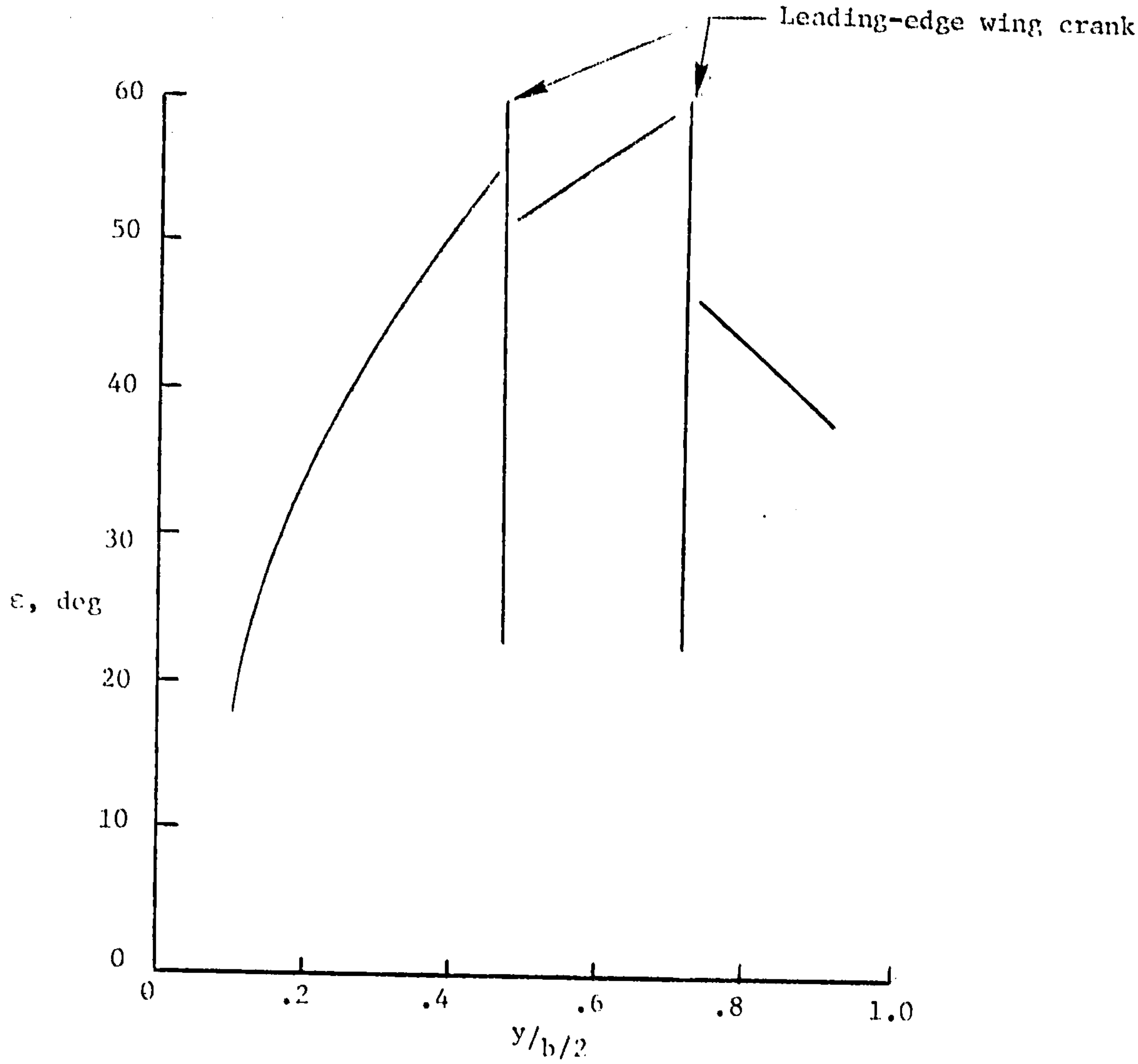

Figure 10.- Variation of theoretical upwash with nondimensional semispan. Theory based on vortex-lattice computational model. α=10° (ref. 5).

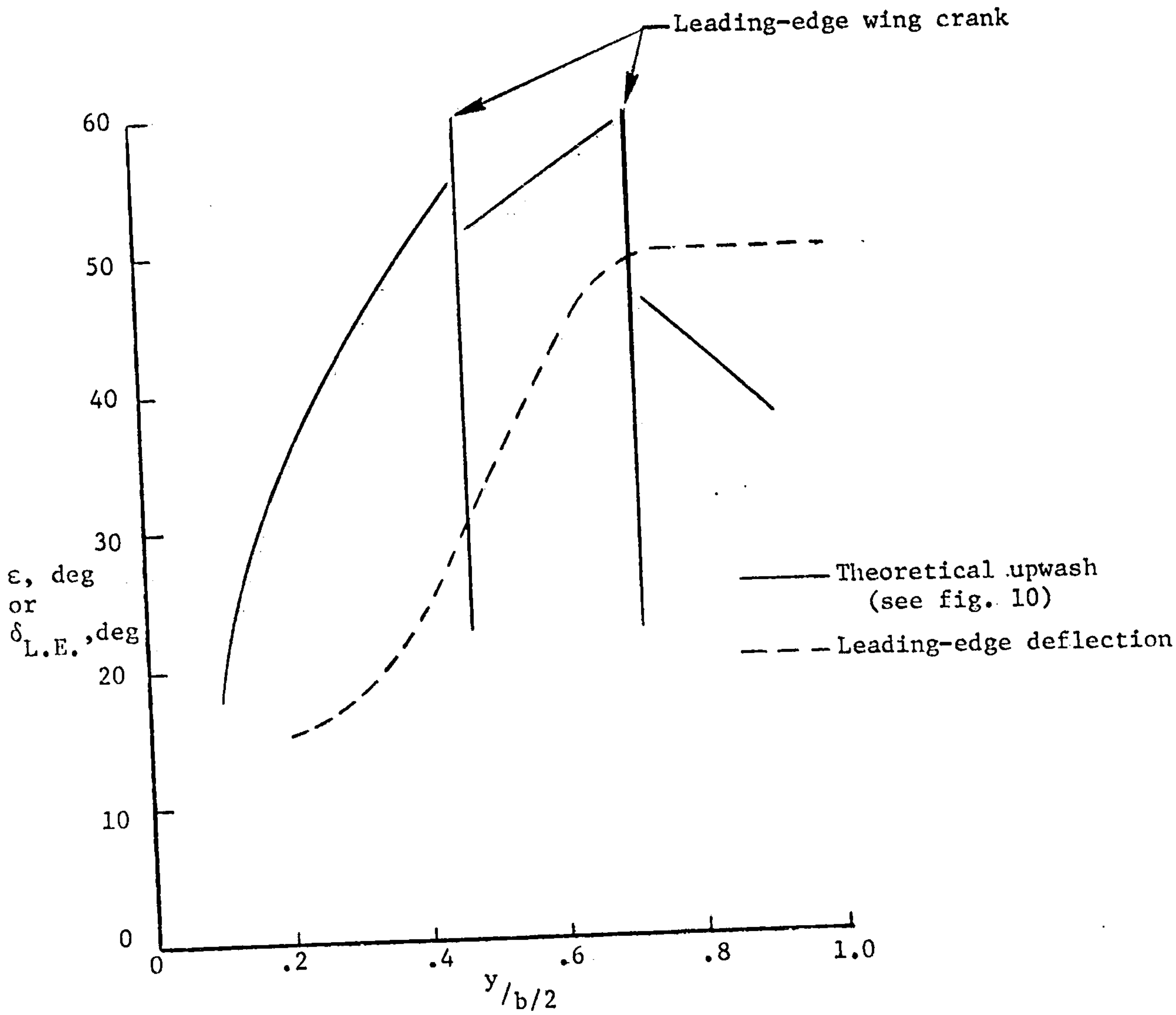

Figure 11.- Comparison of theoretical upwash with optimized leading-edge deflection.

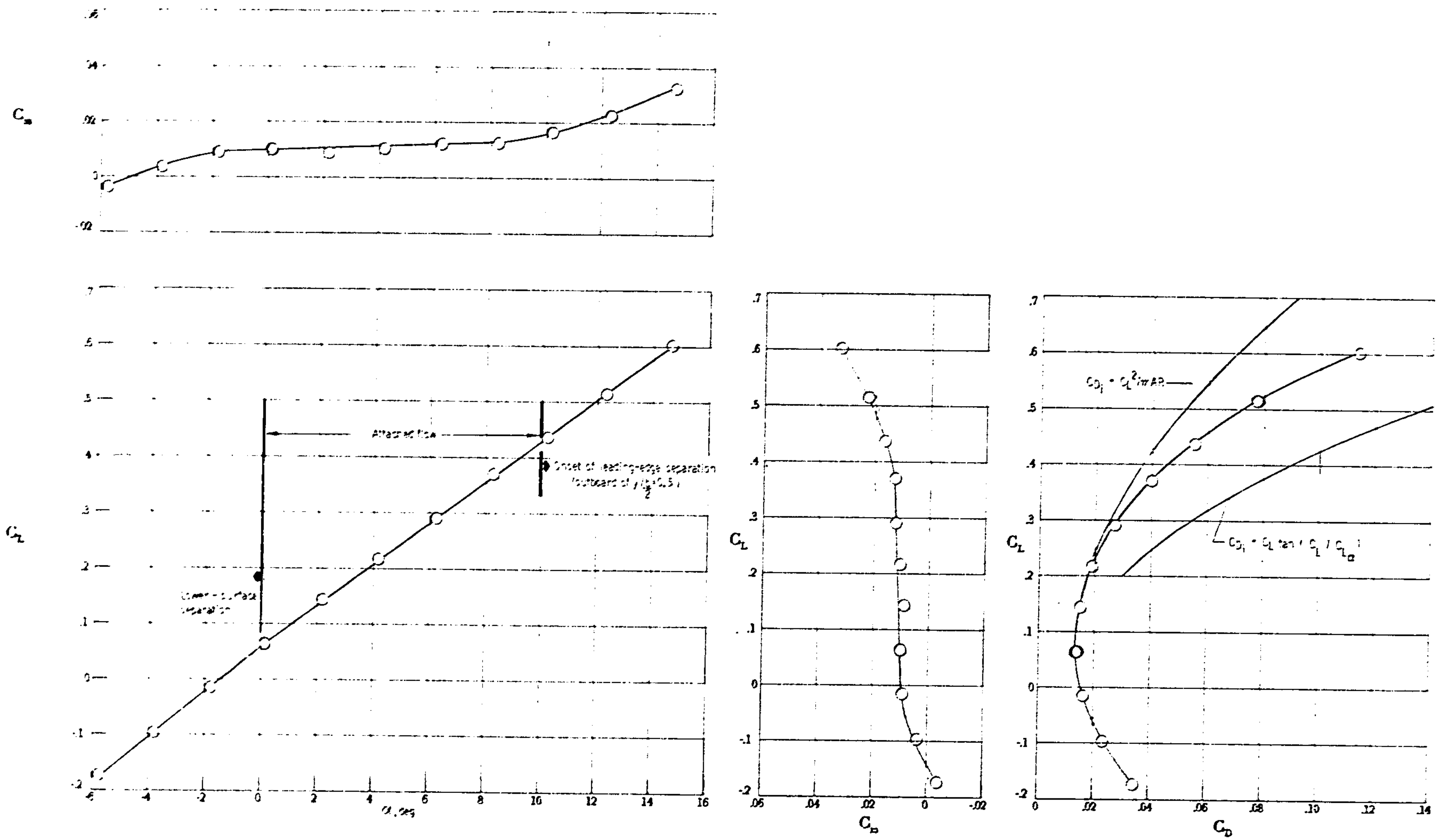

Figure 12.- Longitudinal aerodynamic characteristics for configuration with $\delta_{L.E.} = 16^\circ - 50^\circ$.

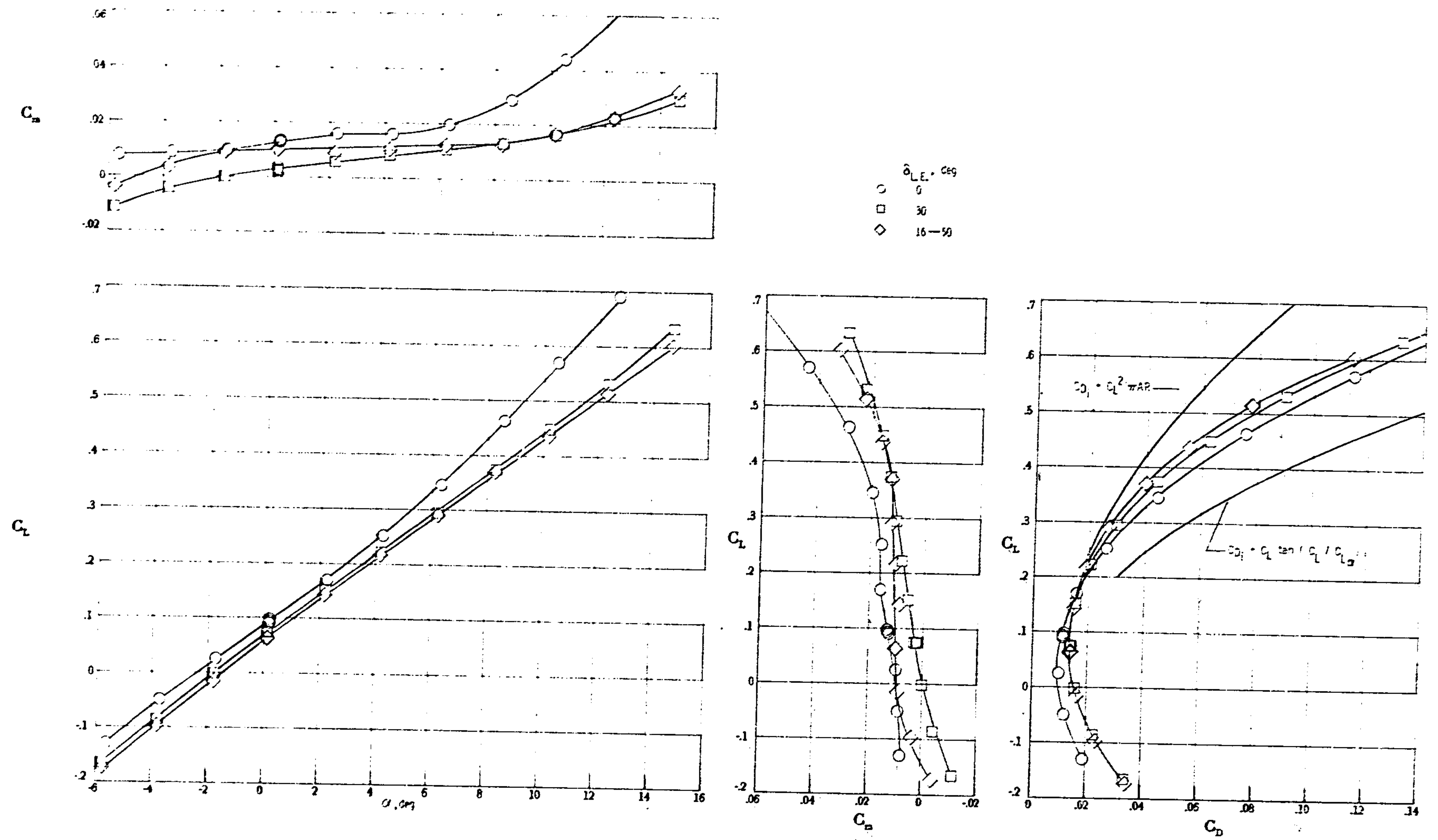

Figure 13.- Effect of wing leading-edge deflection on longitudinal aerodynamic characteristics.

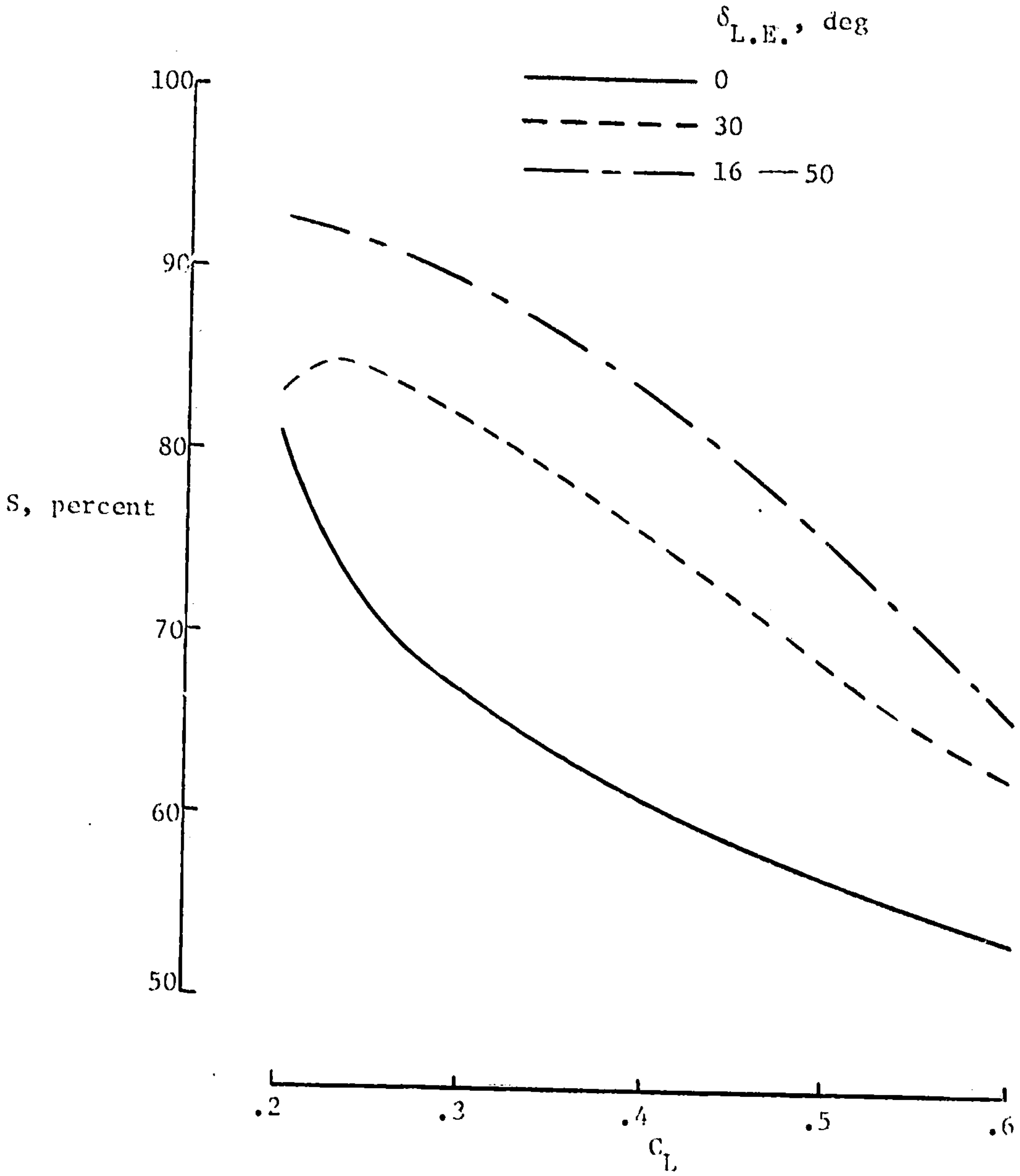

Figure 14.- Effect of continuously warped leading-edge deflection on leading-edge suction.

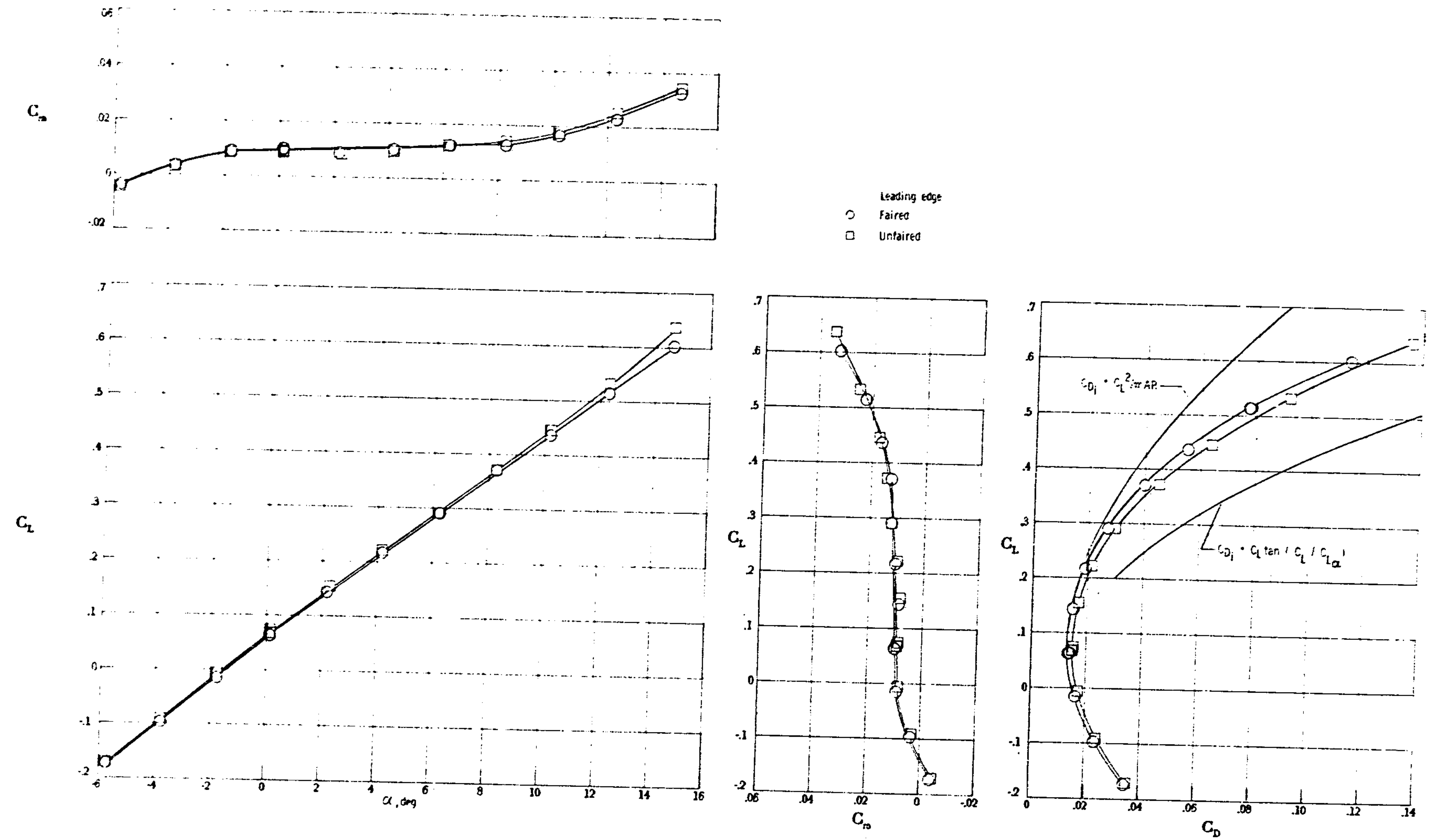

Figure 15.- Effect of removing fairings between adjacent segments of continuously-warped leading-edge. $\delta_{L.E.} = 16^\circ - 50^\circ$.

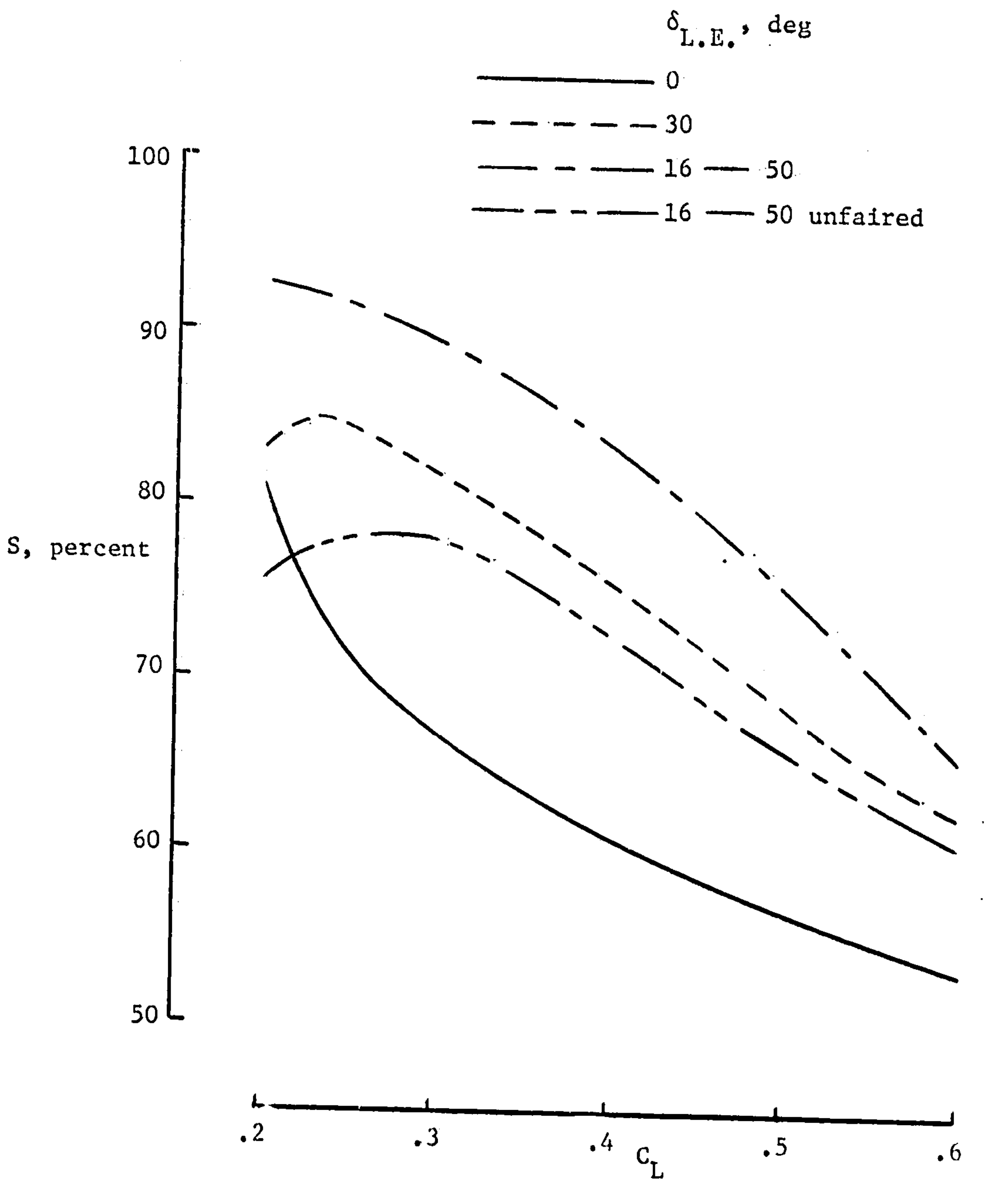

Figure 16.- Effect of removing fairings from adjacent segments of continuously warped leading edge.

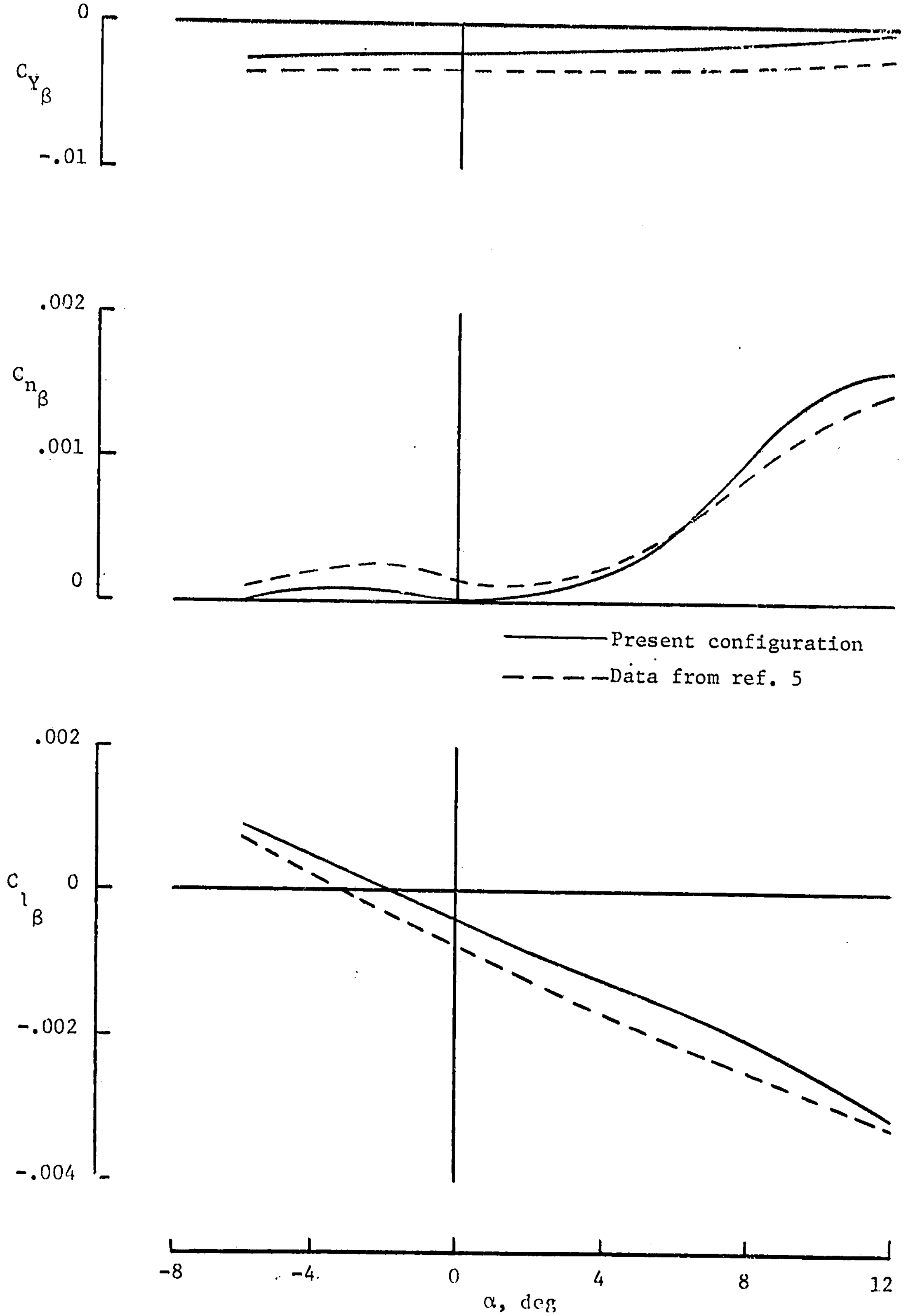

Figure 17.- Variation of lateral-directional stability derivatives with angle of attack. $\delta_{L.E.} = 0°$.

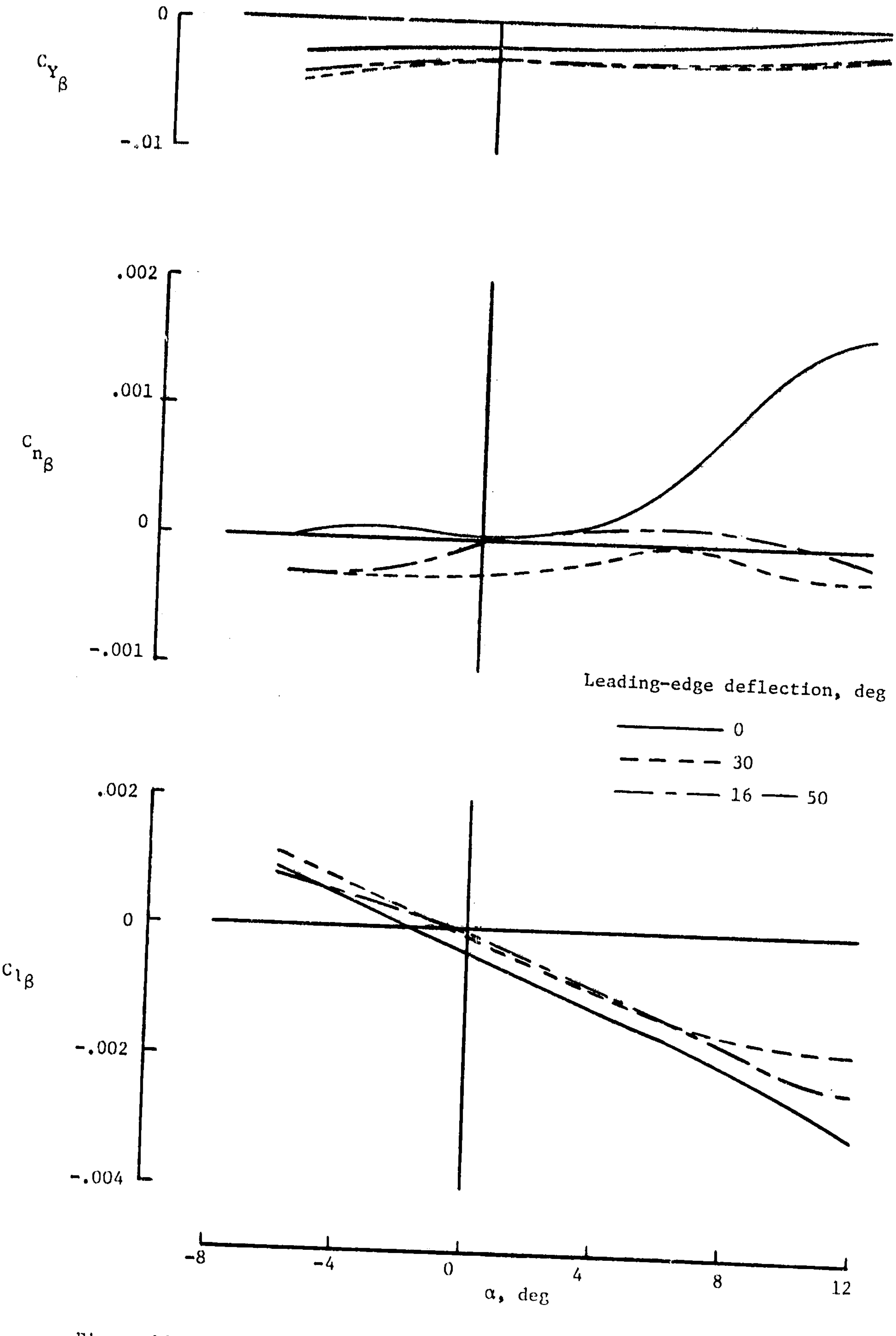

Figure 18.- Effect of leading-edge deflection on lateral-directional stability derivatives.

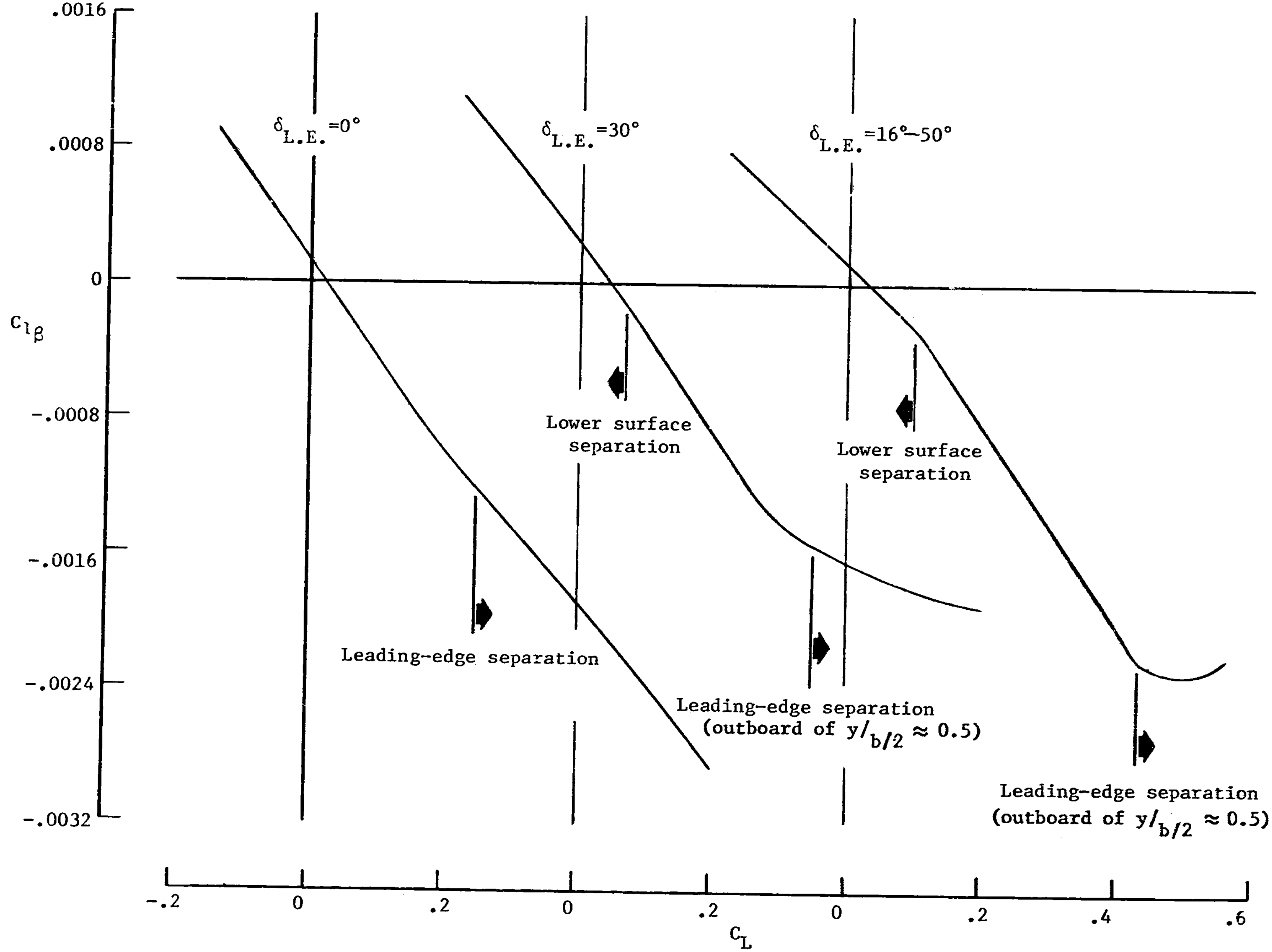

Figure 19.- Effect of leading-edge deflection on C_{l_β} versus C_L.

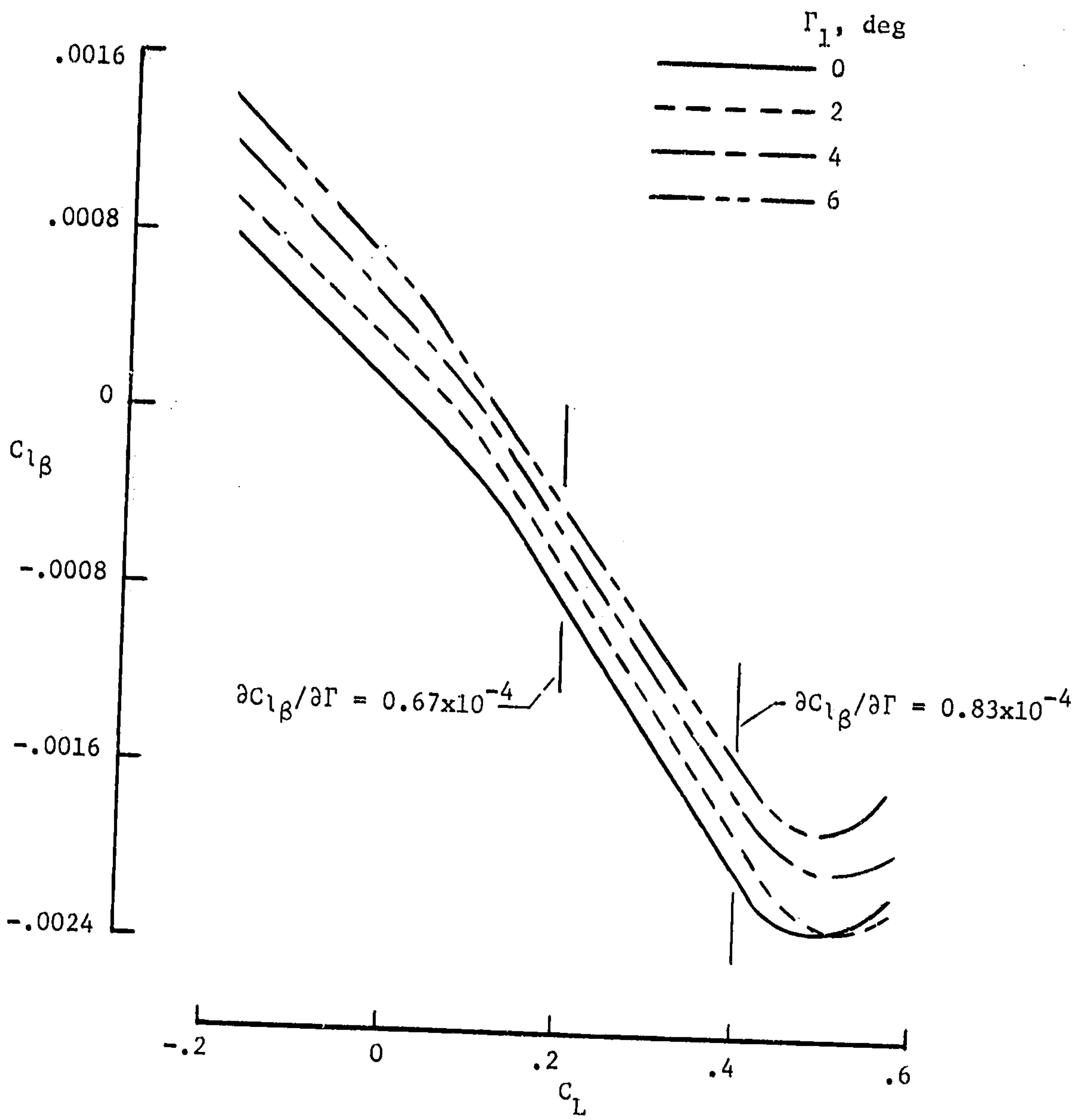

(a) Γ_1 varied, $\Gamma_2 = 0°$

Figure 20.- Effect of geometric anhedral on C_{l_β}.

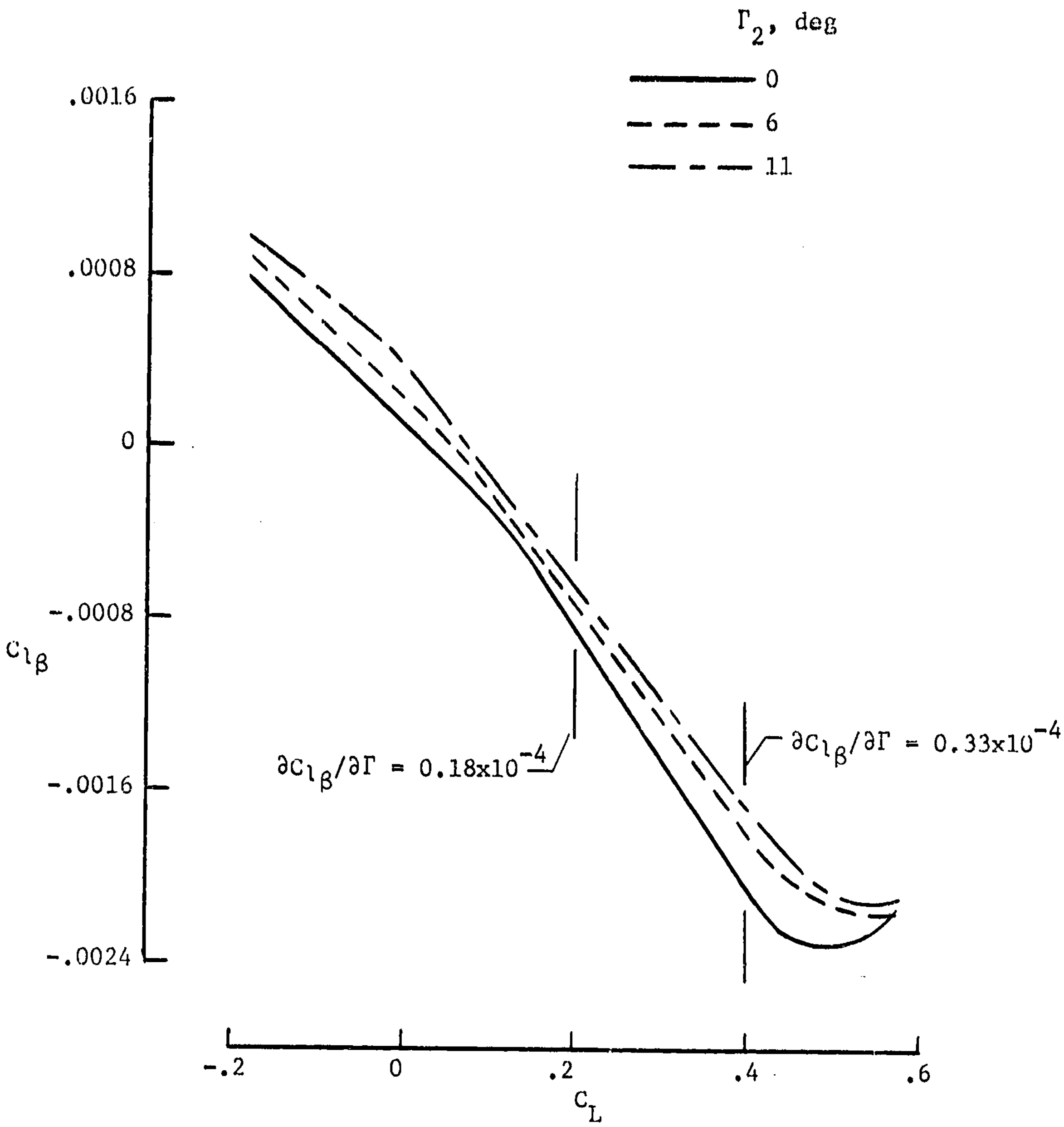

(b) $\Gamma_1 = 0°, \Gamma_2$ = varied

Figure 20.- Concluded.

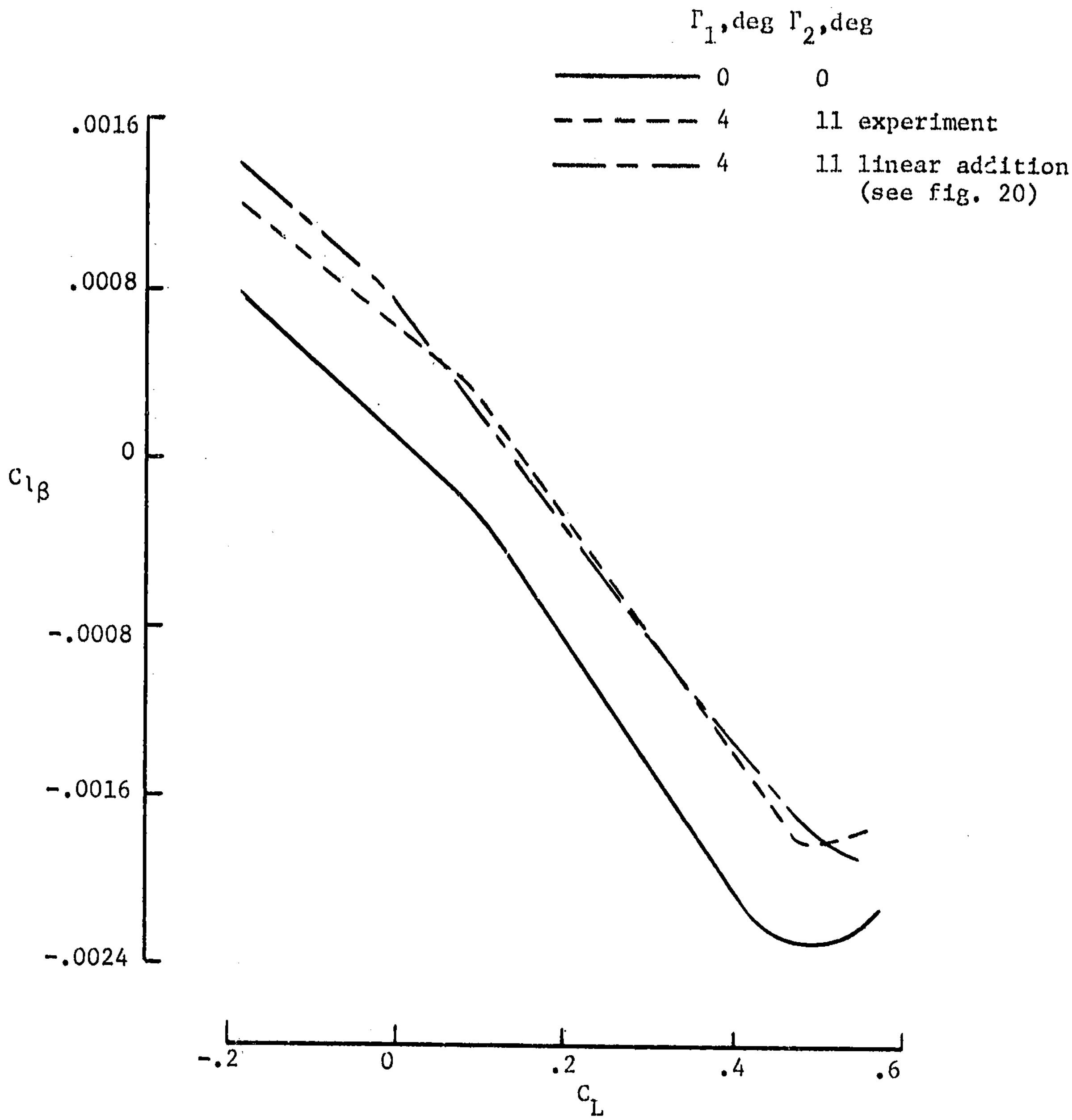

Figure 21.- Effect of geometric anhedral, Γ_1 and Γ_2 in combination, on C_{l_β}.

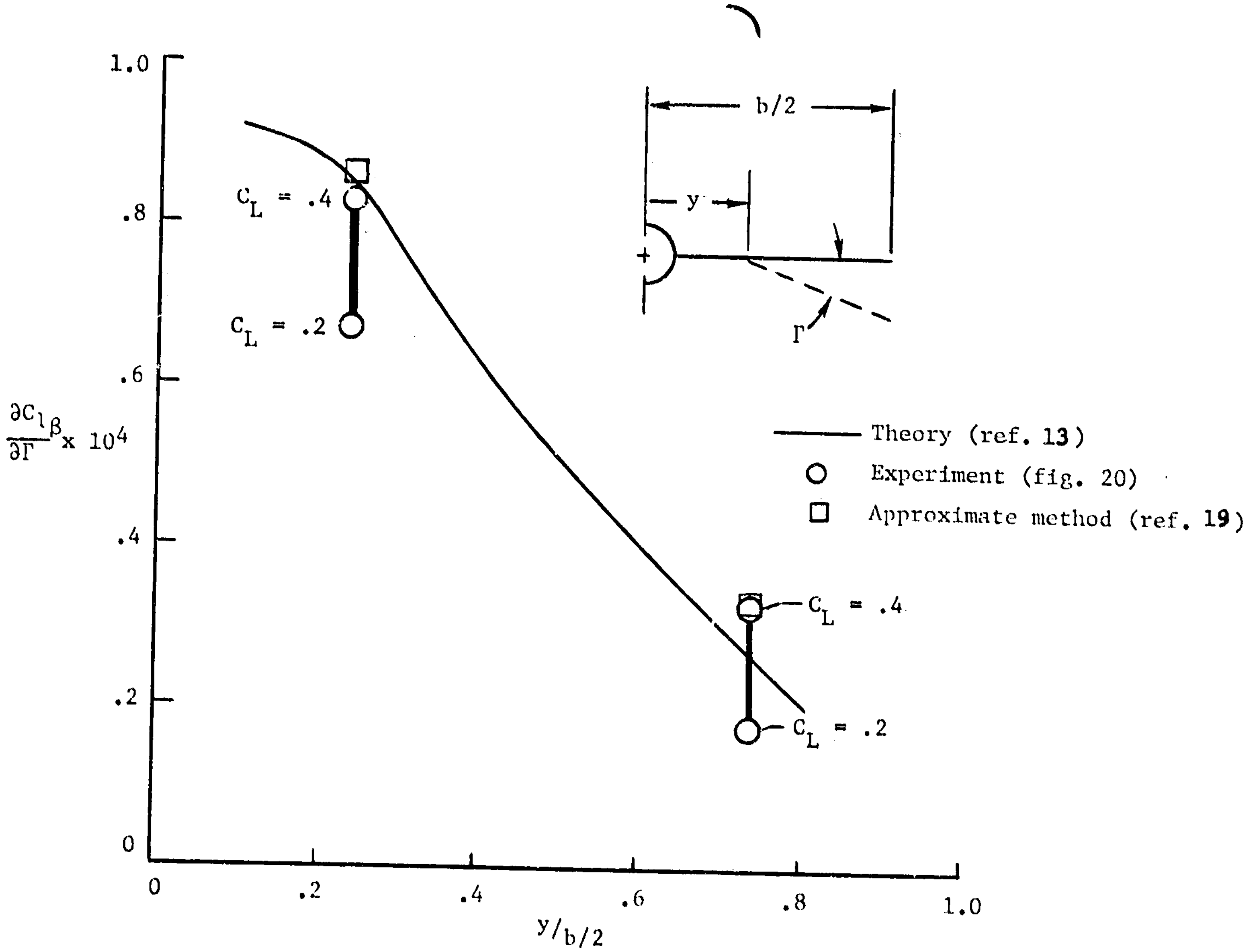

Figure 22.- Values for $\partial C_{l_\beta}/\partial \Gamma$ obtained by inclusion of additional geometric anhedral at span station $y/_{b/2}$.

DATA SUPPLEMENT

The symbols used in the data tabulation are defined as follows:

ALPHA	angle of attack, deg
BETA	angle of sideslip, deg
CD	drag-force coefficient; stability axis
CL	lift-force coefficient; stability axis
CM	pitching-moment coefficient; stability axis
CRM	rolling-moment coefficient; body axis
CY	side-force coefficient; body axis
CYM	yawing-moment coefficient; body axis

TABLE S-1 TEST PROGRAM

Run	β, deg	$\delta_{L.E.}$, deg	Γ_1, deg	Γ_2, deg
1	0	0	0	0
2	5			
3	-5			
4	-5	30		
5	5			
6	0			
12	0	16-50		
13	5			
14	-5			
18	0		6	
19	5			
20	-5			
21	-5		4	
22	5			
23	0			
24	0			11
25	5			
26	-5			
27	-5		2	0
28	5			
29	0			
30	0		0	11
31	5			
32	-5			
33	-5			6
34	5			
35	0			
39	0	16-50 unfaired		0

ORIGINAL PAGE IS OF POOR QUALITY

TABLE S-2.- TABULATED DATA

NASA LANGLEY — 7 X 10 HIGH SPEED TUNNEL

TEST 59 RUN 1

BETA	ALPHA	CL	CD	CM	CRM	CYM	CY
-.06	.17	.0906	.0110	.0128	-.0003	-.0003	.0009
-.08	-5.64	-.1296	.0189	.0078	-.0010	-.0005	.0018
-.08	-3.72	-.0493	.0118	.0088	-.0006	-.0005	.0015
-.07	-1.72	.0256	.0097	.0098	-.0003	-.0003	.0010
-.06	.19	.0939	.0110	.0131	.0003	-.0003	.0014
-.06	2.25	.1700	.0156	.0160	.0000	-.0002	.0015
-.05	4.25	.2521	.0260	.0160	.0001	-.0000	.0006
-.05	6.34	.3456	.0442	.0198	.0003	.0002	.0008
-.04	8.57	.4633	.0754	.0290	.0008	.0005	.0025
-.04	10.51	.5700	.1142	.0441	.0001	.0011	.0034
-.03	12.69	.6907	.1667	.0625	-.0001	.0014	.0048
-.03	14.74	.8019	.2251	.0850	-.0008	.0016	.0064
-.03	15.10	.8195	.2356	.0893	-.0007	.0016	.0065
-.07	.19	.0978	.0114	.0133	-.0001	-.0002	.0025

TEST 59 RUN 2

BETA	ALPHA	CL	CD	CM	CRM	CYM	CY
4.90	.15	.0926	.0107	.0130	-.0031	.0001	-.0101
4.92	-5.72	-.1304	.0193	.0054	.0031	-.0004	-.0113
4.91	-3.75	-.0468	.0117	.0074	.0020	-.0001	-.0100
4.91	-1.75	.0268	.0095	.0092	-.0006	.0001	-.0094
4.90	.17	.0956	.0108	.0134	-.0032	.0002	-.0099
4.88	2.23	.1706	.0158	.0159	-.0048	.0004	-.0099
4.86	4.24	.2568	.0267	.0181	-.0057	.0012	-.0116
4.81	6.33	.3497	.0457	.0229	-.0087	.0033	-.0069
4.77	8.43	.4559	.0742	.0329	-.0111	.0064	-.0048
4.72	10.45	.5507	.1087	.0462	-.0137	.0083	-.0024
4.67	12.67	.6726	.1612	.0655	-.0179	.0089	-.0007
4.61	14.76	.7923	.2228	.0877	-.0209	.0094	-.0010
4.60	15.01	.8022	.2295	.0905	-.0216	.0095	-.0000
4.90	.15	.0996	.0112	.0136	-.0031	.0001	-.0093

TEST 59 RUN 3

BETA	ALPHA	CL	CD	CM	CRM	CYM	CY
-5.02	.24	.0918	.0113	.0123	.0023	-.0005	.0100
-5.08	-5.63	-.1305	.0195	.0052	-.0049	-.0006	.0136
-5.06	-3.64	-.0474	.0122	.0077	-.0028	-.0008	.0120
-5.05	-1.66	.0246	.0102	.0094	-.0001	-.0007	.0106
-5.02	.26	.0921	.0113	.0121	.0024	-.0006	.0098
-4.99	2.32	.1677	.0161	.0147	.0035	-.0005	.0102
-4.96	4.36	.2520	.0270	.0166	.0053	-.0005	.0104
-4.91	6.42	.3476	.0459	.0224	.0065	-.0026	.0078
-4.85	8.54	.4481	.0741	.0318	.0092	-.0043	.0060
-4.79	10.57	.5554	.1111	.0444	.0119	-.0063	.0042
-4.73	12.78	.6732	.1634	.0629	.0143	-.0060	.0051
-4.66	14.86	.7961	.2248	.0839	.0198	-.0056	.0037
-4.65	15.21	.8150	.2359	.0904	.0196	-.0054	.0043
-5.02	.26	.0941	.0116	.0126	.0022	-.0007	.0103

TEST 59 RUN 4

BETA	ALPHA	CL	CD	CM	CRM	CYM	CY
-5.03	.20	.0751	.0141	.0023	.0003	.0008	.0146
-5.10	-5.71	-.1607	.0336	-.0140	-.0061	.0008	.0250
-5.08	-3.72	-.0777	.0221	-.0061	-.0037	.0009	.0213
-5.06	-1.70	.0028	.0158	-.0014	-.0017	.0011	.0172
-5.03	.23	.0784	.0145	.0024	.0001	.0008	.0159
-5.00	2.32	.1564	.0164	.0054	.0031	.0004	.0142
-4.96	4.30	.2282	.0217	.0092	.0053	.0000	.0149
-4.92	6.37	.3049	.0317	.0110	.0073	-.0003	.0162
-4.88	8.45	.3870	.0471	.0130	.0072	.0014	.0158
-4.83	10.37	.4565	.0655	.0173	.0080	.0015	.0129
-4.77	12.53	.5470	.0956	.0237	.0072	.0017	.0129
-4.71	14.51	.6230	.1285	.0323	.0081	.0027	.0150
-4.70	14.65	.6366	.1346	.0333	.0086	.0029	.0143
-5.04	.24	.0886	.0150	.0027	.0003	.0009	.0174

TABLE S-2.- CONTINUED.

NASA LANGLEY ----- 7 X 10 HIGH SPEED TUNNEL

TEST 59 RUN 5

BETA	ALPHA	CL	CD	CM	CRM	CYM	CY
4.91	.11	.0780	.0140	.0026	-.0009	-.0017	-.0133
4.93	-5.79	-.1598	.0336	-.0140	.0048	-.0020	-.0220
4.93	-3.82	-.0789	.0221	-.0066	.0025	-.0019	-.0181
4.92	-1.80	.0026	.0158	-.0006	.0009	-.0019	-.0151
4.91	.14	.0784	.0137	.0027	-.0007	-.0017	-.0138
4.89	2.21	.1543	.0155	.0060	-.0034	-.0011	-.0119
4.87	4.20	.2264	.0209	.0089	-.0050	-.0011	-.0134
4.83	6.27	.2987	.0290	.0121	-.0065	-.0000	-.0128
4.80	8.30	.3754	.0428	.0154	-.0081	-.0003	-.0108
4.76	10.27	.4534	.0626	.0164	-.0102	-.0006	-.0110
4.71	12.47	.5450	.0939	.0223	-.0089	-.0008	-.0097
4.65	14.64	.6223	.1284	.0332	-.0107	.0004	-.0101
4.91	.12	.0780	.0141	.0022	-.0010	-.0018	-.0134

TEST 59 RUN 6

BETA	ALPHA	CL	CD	CM	CRM	CYM	CY
-.06	.11	.0738	.0137	.0027	-.0002	-.0003	.0015
-.08	-5.76	-.1653	.0340	-.0114	-.0010	-.0006	.0029
-.08	-3.79	-.0854	.0226	-.0042	-.0008	-.0004	.0026
-.07	-1.78	-.0013	.0156	.0001	-.0002	-.0004	.0014
-.06	.13	.0750	.0135	.0023	-.0002	-.0003	.0015
-.06	2.20	.1516	.0153	.0058	.0000	-.0004	.0016
-.05	4.19	.2224	.0206	.0084	.0010	-.0004	.0019
-.04	6.24	.2945	.0296	.0107	.0013	-.0005	.0022
-.04	8.31	.3744	.0439	.0131	.0005	.0002	.0016
-.04	10.24	.4488	.0627	.0165	-.0011	.0010	.0033
-.04	12.36	.5316	.0897	.0227	-.0012	.0022	.0064
-.03	14.68	.6338	.1318	.0296	-.0030	.0033	.0031
-.06	.11	.0750	.0140	.0033	-.0001	-.0003	.0015

TEST 59 RUN 12

BETA	ALPHA	CL	CD	CM	CRM	CYM	CY
-.06	.11	.0632	.0138	.0101	.0009	-.0001	.0011
-.08	-5.75	-.1733	.0347	-.0038	-.0002	.0001	.0012
-.08	-3.81	-.0968	.0235	.0036	.0002	.0004	.0011
-.07	-1.78	-.0151	.0164	.0091	.0007	.0002	.0007
-.06	.12	.0629	.0135	.0100	.0007	-.0001	.0008
-.06	2.18	.1432	.0149	.0089	.0009	-.0002	.0019
-.05	4.17	.2168	.0190	.0105	.0006	-.0003	.0019
-.05	6.23	.2905	.0269	.0123	.0011	-.0007	.0023
-.04	8.28	.3703	.0399	.0127	.0009	.0001	.0034
-.04	10.21	.4366	.0552	.0166	.0002	.0014	.0060
-.03	12.33	.5145	.0773	.0227	.0003	.0007	.0076
-.04	12.32	.5144	.0776	.0228	-.0000	.0006	.0085
-.02	14.64	.6022	.1138	.0327	.0012	.0003	.0078
-.06	.12	.0640	.0140	.0100	.0011	-.0001	.0008

TEST 59 RUN 13

BETA	ALPHA	CL	CD	CM	CRM	CYM	CY
4.90	.10	.0651	.0142	.0095	.0004	.0001	-.0136
4.93	-5.87	-.1744	.0350	-.0066	.0040	-.0012	-.0199
4.93	-3.90	-.0967	.0237	.0016	.0027	-.0013	-.0165
4.92	-1.89	-.0137	.0167	.0070	.0011	-.0010	-.0135
4.90	.06	.0620	.0141	.0099	.0009	.0001	-.0140
4.88	2.09	.1410	.0146	.0103	-.0022	.0002	-.0131
4.86	4.11	.2157	.0187	.0113	-.0050	-.0000	-.0140
4.83	6.15	.2932	.0267	.0116	-.0064	.0008	-.0149
4.80	8.20	.3621	.0381	.0143	-.0087	.0007	-.0123
4.76	10.16	.4393	.0555	.0170	-.0110	-.0001	-.0108
4.71	12.30	.5243	.0823	.0237	-.0111	-.0011	-.0066
4.65	14.62	.6164	.1188	.0352	-.0122	-.0019	.0015
4.90	.01	.0620	.0143	.0097	.0007	.0001	-.0131

NASA LANGLEY

7 X 10 HIGH SPEED TUNNEL

TEST 59 RUN 14

BETA	ALPHA	CL	CD	CM	CRM	CYM	CY
-5.03	.20	.0656	.0143	.0084	.0005	-.0001	.0135
-5.09	-5.73	-.1703	.0346	-.0067	-.0036	.0012	.0206
-5.08	-3.75	-.0906	.0234	.0009	-.0020	.0013	.0168
-5.06	-1.74	-.0113	.0166	.0066	-.0005	.0008	.0142
-5.03	.16	.0649	.0141	.0082	.0006	-.0001	.0133
-5.00	2.26	.1455	.0154	.0087	.0028	-.0006	.0129
-4.96	4.28	.2178	.0196	.0108	.0051	-.0007	.0142
-4.92	6.31	.2934	.0280	.0122	.0068	-.0007	.0158
-4.87	8.37	.3678	.0404	.0137	.0088	-.0004	.0158
-4.82	10.31	.4386	.0560	.0167	.0110	-.0001	.0127
-4.76	12.44	.5202	.0813	.0232	.0103	.0008	.0117
-4.69	14.81	.6289	.1241	.0331	.0066	.0005	.0095
-5.03	.19	.0670	.0144	.0087	.0001	-.0001	.0142

TEST 59 RUN 16

BETA	ALPHA	CL	CD	CM	CRM	CYM	CY
-.07	.13	.0686	.0145	.0103	.0002	.0001	.0014
-.09	-5.70	-.1606	.0344	-.0027	-.0003	.0005	.0022
-.08	-3.76	-.0811	.0237	.0036	.0006	.0007	.0014
-.07	-1.77	-.0034	.0171	.0083	.0006	.0006	.0009
-.07	.18	.0737	.0146	.0101	.0003	.0001	.0020
-.06	2.23	.1539	.0163	.0097	.0006	-.0001	.0025
-.05	4.22	.2262	.0210	.0116	.0004	-.0002	.0029
-.05	6.26	.2987	.0292	.0131	.0006	-.0003	.0044
-.04	8.30	.3773	.0426	.0136	.0007	.0001	.0044
-.04	10.24	.4445	.0583	.0185	.0002	.0013	.0075
-.04	12.37	.5186	.0806	.0253	-.0000	.0009	.0082
-.03	14.63	.6026	.1142	.0344	.0001	-.0002	.0089
-.07	.15	.0791	.0153	.0103	.0003	.0001	.0032

TEST 59 RUN 19

BETA	ALPHA	CL	CD	CM	CRM	CYM	CY
4.90	.16	.0676	.0145	.0099	.0030	.0005	-.0166
4.93	-5.79	-.1655	.0344	-.0050	.0067	-.0007	-.0242
4.93	-3.82	-.0865	.0234	.0012	.0052	-.0008	-.0205
4.92	-1.81	-.0085	.0169	.0069	.0040	-.0004	-.0174
4.90	.10	.0651	.0146	.0099	.0028	.0005	-.0159
4.88	2.18	.1429	.0156	.0112	.0000	.0009	-.0155
4.86	4.19	.2160	.0196	.0125	-.0025	.0009	-.0160
4.83	6.23	.2906	.0274	.0125	-.0044	.0016	-.0170
4.80	8.27	.3605	.0387	.0166	-.0065	.0012	-.0164
4.76	10.23	.4359	.0558	.0204	-.0089	.0005	-.0142
4.71	12.35	.5141	.0811	.0266	-.0097	-.0011	-.0094
4.65	14.61	.6136	.1196	.0364	-.0087	-.0016	-.0029
4.90	.10	.0650	.0146	.0098	.0032	.0006	-.0168

TEST 59 RUN 20

BETA	ALPHA	CL	CD	CM	CRM	CYM	CY
-5.03	.18	.0616	.0142	.0085	-.0019	-.0002	.0136
-5.09	-5.71	-.1693	.0348	-.0050	-.0055	.0016	.0211
-5.08	-3.72	-.0903	.0236	.0014	-.0040	.0016	.0170
-5.06	-1.73	-.0140	.0170	.0067	-.0032	.0008	.0149
-5.03	.21	.0645	.0144	.0086	-.0015	-.0001	.0140
-5.00	2.25	.1414	.0155	.0094	.0012	-.0007	.0132
-4.96	4.27	.2124	.0196	.0116	.0031	-.0009	.0141
-4.92	6.31	.2850	.0274	.0130	.0043	-.0011	.0162
-4.88	8.36	.3595	.0392	.0160	.0058	-.0006	.0173
-4.82	10.31	.4330	.0558	.0193	.0088	-.0009	.0144
-4.76	12.46	.5129	.0800	.0251	.0084	.0001	.0126
-4.69	14.78	.6129	.1193	.0325	.0051	.0013	.0103
-5.03	.19	.0661	.0144	.0084	-.0016	-.0001	.0130

ORIGINAL PAGE IS OF POOR QUALITY

TABLE S-2.- CONTINUED.

NASA LANGLEY 7 X 10 HIGH SPEED TUNNEL

TEST 59 RUN 21

BETA	ALPHA	CL	CD	CM	CRM	CYM	CY
-5.03	.19	.0675	.0142	.0083	-.0014	-.0001	.0151
-5.10	-5.70	-.1617	.0337	-.0065	-.0044	.0017	.0220
-5.08	-3.71	-.0826	.0228	.0008	-.0035	.0018	.0178
-5.06	-1.70	-.0032	.0164	.0061	-.0022	.0009	.0157
-5.03	.21	.0713	.0144	.0081	-.0011	-.0001	.0157
-5.00	2.26	.1518	.0161	.0092	.0014	-.0007	.0150
-4.96	4.28	.2250	.0207	.0114	.0035	-.0008	.0169
-4.92	6.31	.2973	.0288	.0119	.0046	-.0010	.0182
-4.88	8.42	.3740	.0418	.0157	.0064	-.0005	.0196
-4.82	10.34	.4475	.0585	.0181	.0098	-.0005	.0152
-4.76	12.48	.5272	.0835	.0242	.0095	.0004	.0128
-4.69	14.82	.6309	.1251	.0323	.0062	.0009	.0101
-5.03	.22	.0774	.0148	.0081	-.0009	.0001	.0165

TEST 59 RUN 22

BETA	ALPHA	CL	CD	CM	CRM	CYM	CY
4.90	.11	.0688	.0143	.0093	.0017	.0003	-.0145
4.93	-5.77	-.1639	.0337	-.0058	.0058	-.0010	-.0217
4.93	-3.79	-.0952	.0231	.0019	.0040	-.0011	-.0179
4.92	-1.78	-.0030	.0162	.0070	.0028	-.0006	-.0156
4.90	.14	.0686	.0141	.0090	.0019	.0004	-.0146
4.88	2.21	.1482	.0153	.0104	-.0009	.0007	-.0139
4.86	4.25	.2251	.0193	.0121	-.0033	.0007	-.0152
4.83	6.27	.2971	.0276	.0121	-.0056	.0012	-.0146
4.80	8.32	.3711	.0397	.0160	-.0074	.0012	-.0157
4.76	10.30	.4451	.0576	.0183	-.0095	.0007	-.0121
4.71	12.40	.5232	.0836	.0253	-.0098	-.0009	-.0085
4.65	14.62	.6118	.1185	.0371	-.0109	-.0019	-.0013
4.90	.15	.0733	.0144	.0101	.0015	.0003	-.0140

TEST 59 RUN 23

BETA	ALPHA	CL	CD	CM	CRM	CYM	CY
-.06	.11	.0620	.0134	.0092	.0005	.0001	-.0000
-.08	-5.76	-.1710	.0341	-.0026	-.0002	.0004	.0004
-.08	-3.79	-.0935	.0230	.0042	.0003	.0004	.0000
-.07	-1.78	-.0125	.0162	.0087	.0005	.0003	.0003
-.06	.14	.0640	.0137	.0092	.0007	.0002	.0003
-.06	2.22	.1460	.0146	.0091	.0007	-.0001	.0004
-.05	4.18	.2165	.0188	.0108	.0004	-.0001	.0008
-.04	6.22	.2858	.0264	.0124	.0011	-.0003	.0010
-.04	8.33	.3708	.0397	.0133	.0007	.0002	.0021
-.04	10.30	.4377	.0550	.0177	.0002	.0015	.0041
-.03	12.33	.5078	.0763	.0239	-.0001	.0004	.0057
-.02	14.62	.5914	.1102	.0336	.0015	-.0004	.0028
-.06	.12	.0635	.0132	.0092	-.0000	.0001	.0005

TEST 59 RUN 24

BETA	ALPHA	CL	CD	CM	CRM	CYM	CY
-.06	.13	.0674	.0139	.0096	.0006	.0000	.0009
-.08	-5.70	-.1557	.0320	-.0060	-.0004	.0001	.0014
-.08	-3.77	-.0843	.0224	.0027	-.0002	.0001	.0019
-.07	-1.78	-.0071	.0163	.0078	.0003	.0002	.0013
-.07	.13	.0693	.0138	.0094	.0005	.0000	.0011
-.06	2.21	.1505	.0153	.0095	.0002	-.0003	.0025
-.05	4.18	.2189	.0195	.0110	.0005	-.0003	.0022
-.05	6.25	.2943	.0276	.0144	.0006	-.0002	.0025
-.04	8.30	.3686	.0409	.0151	.0006	.0001	.0036
-.04	10.22	.4370	.0565	.0199	.0001	.0013	.0062
-.03	12.33	.5085	.0782	.0270	-.0005	.0006	.0075
-.02	14.63	.5960	.1113	.0371	.0005	-.0010	.0076
-.07	.15	.0742	.0140	.0101	.0005	.0001	.0022

TABLE S-2.- CONTINUED.

NASA LANGLEY 7 X 10 HIGH SPEED TUNNEL

TEST 59 RUN 25

BETA	ALPHA	CL	CD	CM	CRM	CYM	CY
4.90	.10	.0637	.0138	.0088	.0037	.0017	-.0190
4.93	-5.78	-.1591	.0325	-.0082	.0061	-.0006	-.0228
4.93	-3.83	-.0852	.0226	-.0001	.0052	-.0006	-.0194
4.92	-1.62	-.0076	.0163	.0062	.0043	.0004	-.0181
4.90	.09	.0636	.0137	.0090	.0036	.0019	-.0191
4.88	2.16	.1421	.0149	.0111	.0011	.0020	-.0179
4.86	4.16	.2145	.0168	.0130	-.0018	.0015	-.0185
4.83	6.24	.2900	.0272	.0133	-.0036	.0026	-.0185
4.80	8.28	.3629	.0392	.0161	-.0063	.0024	-.0171
4.76	10.28	.4383	.0566	.0222	-.0081	.0019	-.0161
4.71	12.35	.5120	.0815	.0280	-.0075	.0008	-.0141
4.65	14.60	.6003	.1163	.0409	-.0092	-.0001	-.0052
4.90	.09	.0658	.0139	.0090	.0031	.0017	-.0179

TEST 59 RUN 26

BETA	ALPHA	CL	CD	CM	CRM	CYM	CY
-5.03	.19	.0635	.0138	.0081	-.0024	-.0016	.0171
-5.09	-5.70	-.1617	.0327	-.0100	-.0053	.0010	.0225
-5.08	-3.72	-.0857	.0225	-.0004	-.0040	.0010	.0185
-5.05	-1.71	-.0068	.0161	.0051	-.0027	.0000	.0168
-5.03	.20	.0616	.0138	.0080	-.0022	-.0015	.0168
-5.00	2.26	.1403	.0148	.0099	-.0000	-.0019	.0160
-4.96	4.30	.2138	.0194	.0114	.0026	-.0019	.0166
-4.92	6.31	.2870	.0273	.0136	.0040	-.0020	.0175
-4.88	8.38	.3613	.0399	.0172	.0053	-.0016	.0201
-4.81	10.44	.4369	.0569	.0209	.0082	-.0019	.0154
-4.76	12.46	.5092	.0798	.0271	.0091	-.0016	.0139
-4.69	14.79	.6122	.1194	.0370	.0062	.0001	.0089
-5.03	.21	.0654	.0139	.0087	-.0025	-.0016	.0170

TEST 59 RUN 27

BETA	ALPHA	CL	CD	CM	CRM	CYM	CY
-5.03	.19	.0703	.0141	.0070	-.0008	-.0001	.0131
-5.09	-5.71	-.1632	.0339	-.0075	-.0046	.0015	.0210
-5.08	-3.73	-.0860	.0230	.0010	-.0028	.0016	.0159
-5.06	-1.71	-.0045	.0164	.0062	-.0015	.0010	.0144
-5.03	.24	.0740	.0142	.0077	-.0004	-.0003	.0131
-5.00	2.27	.1531	.0156	.0086	.0015	-.0005	.0139
-4.96	4.30	.2264	.0202	.0102	.0040	-.0007	.0142
-4.92	6.33	.3017	.0289	.0121	.0050	-.0006	.0165
-4.88	8.41	.3770	.0417	.0137	.0070	-.0002	.0166
-4.82	10.34	.4462	.0577	.0161	.0093	-.0004	.0129
-4.76	12.49	.5279	.0830	.0225	.0101	.0001	.0106
-4.69	14.83	.6362	.1255	.0330	.0062	.0004	.0081
-5.03	.22	.0775	.0145	.0077	-.0005	-.0001	.0139

TEST 59 RUN 28

BETA	ALPHA	CL	CD	CM	CRM	CYM	CY
4.90	.10	.0668	.0141	.0091	.0013	.0003	-.0140
4.93	-5.80	-.1659	.0341	-.0066	.0044	-.0010	-.0202
4.92	-3.64	-.0884	.0234	.0016	.0033	-.0012	-.0164
4.92	-1.84	-.0076	.0168	.0065	.0019	-.0007	-.0143
4.90	.09	.0673	.0141	.0088	.0015	.0003	-.0141
4.88	2.17	.1476	.0151	.0104	-.0013	.0006	-.0135
4.86	4.17	.2190	.0189	.0110	-.0044	.0004	-.0142
4.83	6.22	.2981	.0271	.0115	-.0065	.0008	-.0146
4.80	8.27	.3698	.0389	.0137	-.0088	.0008	-.0149
4.76	10.23	.4433	.0566	.0157	-.0113	.0005	-.0113
4.71	12.39	.5234	.0826	.0224	-.0112	-.0008	-.0088
4.65	14.62	.6111	.1174	.0253	-.0127	-.0013	-.0009
4.90	.09	.0672	.0141	.0089	.0010	.0002	-.0142

TABLE S-2.- CONTINUED.

NASA LANGLEY 7 X 10 HIGH SPEED TUNNEL

TEST 59 RUN 29

BETA	ALPHA	CL	CD	CM	CRM	CYM	CY
-.06	.12	.0656	.0138	.0091	.0007	-.0001	-.0001
-.08	-5.76	-.1721	.0345	-.0041	-.0004	.0003	.0008
-.08	-3.80	-.0921	.0233	.0037	-.0005	.0002	.0009
-.07	-1.78	-.0116	.0164	.0076	.0007	.0002	.0002
-.06	.14	.0668	.0138	.0097	.0007	-.0000	.0007
-.06	2.18	.1474	.0147	.0079	.0003	-.0001	.0010
-.05	4.20	.2193	.0189	.0094	.0002	-.0003	.0006
-.04	6.22	.2925	.0267	.0109	.0001	-.0004	.0018
-.04	8.29	.3692	.0397	.0114	.0001	-.0000	.0024
-.04	10.24	.4393	.0555	.0157	-.0006	.0013	.0051
-.03	12.40	.5176	.0784	.0220	-.0009	.0003	.0070
-.02	14.63	.5997	.1116	.0310	.0002	-.0006	.0061
-.06	.12	.0641	.0138	.0089	.0006	-.0001	-.0002

TEST 59 RUN 30

BETA	ALPHA	CL	CD	CM	CRM	CYM	CY
-.06	.12	.0659	.0136	.0088	.0002	-.0001	.0009
-.08	-5.73	-.1628	.0333	-.0085	-.0005	.0002	.0015
-.08	-3.78	-.0896	.0230	.0019	.0000	.0002	.0011
-.07	-1.77	-.0084	.0163	.0071	.0007	.0004	.0005
-.06	.15	.0688	.0138	.0090	.0006	-.0000	.0010
-.06	2.20	.1489	.0148	.0082	.0006	-.0002	.0012
-.05	4.26	.2213	.0194	.0101	.0003	-.0003	.0021
-.05	6.25	.2925	.0272	.0131	.0007	-.0001	.0027
-.04	8.30	.3716	.0408	.0127	.0011	.0001	.0023
-.04	10.25	.4395	.0566	.0179	.0002	.0013	.0057
-.03	12.37	.5129	.0781	.0246	-.0002	.0006	.0056
-.02	14.64	.6013	.1132	.0337	.0007	-.0011	.0064
-.06	.15	.0728	.0138	.0102	-.0003	-.0001	.0013

TEST 59 RUN 31

BETA	ALPHA	CL	CD	CM	CRM	CYM	CY
4.90	.09	.0648	.0136	.0081	.0019	.0014	-.0170
4.93	-5.80	-.1613	.0329	-.0097	.0048	-.0006	-.0212
4.92	-3.81	-.0853	.0225	-.0009	.0038	-.0007	-.0182
4.92	-1.79	-.0060	.0160	.0054	.0025	.0001	-.0169
4.90	.15	.0692	.0136	.0088	.0021	.0014	-.0171
4.88	2.18	.1462	.0146	.0096	-.0012	.0013	-.0160
4.86	4.21	.2191	.0186	.0112	-.0038	.0011	-.0167
4.83	6.24	.2950	.0270	.0121	-.0051	.0018	-.0178
4.80	8.32	.3712	.0396	.0153	-.0078	.0016	-.0164
4.76	10.27	.4419	.0569	.0188	-.0090	.0015	-.0148
4.71	12.44	.5249	.0843	.0265	-.0096	.0001	-.0109
4.65	14.63	.6105	.1183	.0377	-.0116	-.0008	-.0016
4.90	.11	.0686	.0136	.0081	.0021	.0013	-.0177

TEST 59 RUN 32

BETA	ALPHA	CL	CD	CM	CRM	CYM	CY
-5.03	.20	.0666	.0140	.0068	-.0010	-.0011	.0159
-5.09	-5.71	-.1613	.0329	-.0107	-.0049	.0008	.0216
-5.08	-3.76	-.0859	.0226	-.0015	-.0033	.0009	.0177
-5.05	-1.72	-.0075	.0161	.0046	-.0015	.0002	.0156
-5.03	.18	.0662	.0138	.0070	-.0009	-.0010	.0157
-5.00	2.26	.1463	.0151	.0088	.0013	-.0014	.0155
-4.96	4.26	.2174	.0192	.0107	.0038	-.0013	.0165
-4.92	6.28	.2906	.0276	.0121	.0054	-.0011	.0175
-4.88	8.37	.3642	.0401	.0150	.0070	-.0007	.0182
-4.82	10.32	.4386	.0565	.0182	.0093	-.0012	.0155
-4.76	12.48	.5206	.0820	.0239	.0099	-.0005	.0141
-4.69	14.80	.6202	.1211	.0350	.0068	.0005	.0085
-5.03	.17	.0660	.0139	.0073	-.0012	-.0011	.0157

TABLE S-2.- CONCLUDED.

NASA LANGLEY   7 X 10 HIGH SPEED TUNNEL

TEST 59   RUN 33

BETA	ALPHA	CL	CD	CM	CRM	CYM	CY
-5.03	.20	.0713	.0143	.0066	-.0002	-.0004	.0142
-5.09	-5.69	-.1583	.0332	-.0099	-.0039	.0011	.0207
-5.08	-3.74	-.0832	.0226	-.0014	-.0025	.0013	.0171
-5.05	-1.71	-.0035	.0163	.0046	-.0008	.0005	.0150
-5.03	.20	.0711	.0141	.0070	-.0005	-.0006	.0149
-5.00	2.30	.1527	.0154	.0076	.0024	-.0007	.0135
-4.96	4.29	.2236	.0201	.0094	.0049	-.0008	.0152
-4.92	6.35	.2978	.0286	.0110	.0061	-.0006	.0158
-4.88	8.41	.3754	.0415	.0141	.0077	-.0002	.0171
-4.82	10.36	.4461	.0580	.0164	.0103	-.0005	.0140
-4.76	12.51	.5278	.0836	.0225	.0101	.0002	.0129
-4.69	14.82	.6275	.1234	.0332	.0074	.0007	.0079
-5.03	.22	.0729	.0142	.0066	-.0003	-.0004	.0146

TEST 59   RUN 34

BETA	ALPHA	CL	CD	CM	CRM	CYM	CY
4.90	.10	.0694	.0137	.0083	.0015	.0007	-.0145
4.93	-5.81	-.1642	.0337	-.0096	.0045	-.0009	-.0196
4.92	-3.84	-.0868	.0230	-.0003	.0033	-.0011	-.0169
4.92	-1.81	-.0064	.0164	.0054	.0020	-.0005	-.0149
4.90	.14	.0722	.0139	.0087	.0017	.0009	-.0147
4.88	2.18	.1510	.0151	.0092	-.0016	.0008	-.0139
4.86	4.20	.2222	.0194	.0101	-.0042	.0006	-.0138
4.83	6.24	.2984	.0274	.0116	-.0055	.0014	-.0152
4.80	8.30	.3691	.0394	.0138	-.0078	.0013	-.0143
4.76	10.26	.4437	.0573	.0169	-.0089	.0010	-.0125
4.71	12.39	.5247	.0836	.0245	-.0097	-.0003	-.0099
4.64	14.63	.6165	.1195	.0369	-.0122	-.0013	.0021
4.90	.08	.0691	.0139	.0080	.0016	.0008	-.0146

TEST 59   RUN 35

BETA	ALPHA	CL	CD	CM	CRM	CYM	CY
-.08	-.04	.0302	.0040	-.0022	-.0006	.0036	.0061
-.08	.05	.0677	.0137	.0086	.0005	.0001	.0016
-.10	-5.81	-.1663	.0340	-.0067	-.0004	.0005	.0019
-.09	-3.86	-.0907	.0231	.0021	.0003	.0004	.0020
-.09	-1.85	-.0093	.0165	.0076	.0005	.0004	.0016
-.08	.09	.0697	.0137	.0087	.0009	.0001	.0017
-.07	2.14	.1520	.0148	.0072	.0008	.0009	.0016
-.07	4.14	.2234	.0194	.0091	.0008	.0000	.0023
-.06	6.18	.2948	.0274	.0109	.0008	.0001	.0030
-.05	8.24	.3745	.0407	.0121	.0012	.0005	.0031
-.06	10.16	.4419	.0558	.0164	-.0001	.0013	.0075
-.05	12.29	.5190	.0766	.0221	.0005	.0006	.0073
-.03	14.59	.6077	.1141	.0328	.0017	-.0004	.0054
-.08	.05	.0677	.0138	.0087	.0007	.0001	.0017

TEST 59   RUN 39

BETA	ALPHA	CL	CD	CM	CRM	CYM	CY
-.07	.12	.0676	.0148	.0094	.0005	-.0001	.0015
-.08	-5.77	-.1706	.0355	-.0046	-.0004	.0001	.0020
-.08	-3.82	-.0912	.0241	.0031	.0001	.0002	.0010
-.07	-1.75	-.0058	.0173	.0086	.0004	.0002	.0016
-.07	.13	.0686	.0149	.0093	.0004	.0000	.0018
-.06	2.28	.1545	.0169	.0084	.0006	-.0002	.0023
-.05	4.18	.2218	.0214	.0098	.0008	-.0001	.0026
-.05	6.19	.2968	.0296	.0123	.0011	-.0001	.0033
-.04	8.26	.3717	.0452	.0143	.0012	.0004	.0020
-.04	10.22	.4458	.0639	.0175	.0005	.0010	.0048
-.04	12.34	.5329	.0921	.0252	-.0000	.0017	.0100
-.02	14.67	.6373	.1361	.0345	.0006	-.0001	.0073
-.07	.13	.0744	.0152	.0089	.0005	-.0000	.0023

1. Report No. TM 80083	2. Government Accession No.	3. Recipient's Catalog No.
4. Title and Subtitle INFLUENCE OF OPTIMIZED LEADING-EDGE DEFLECTION AND GEOMETRIC ANHEDRAL ON THE LOW-SPEED AERODYNAMIC CHARACTERISTICS OF A LOW-ASPECT-RATIO HIGHLY SWEPT ARROW-WING CONFIGURATION		5. Report Date June 1979
		6. Performing Organization Code
7. Author(s) Paul L. Coe, Jr. and Jarrett K. Huffman		8. Performing Organization Report No.
9. Performing Organization Name and Address NASA Langley Research Center Hampton, VA 23665		10. Work Unit No. 517-53-43-02
		11. Contract or Grant No.
12. Sponsoring Agency Name and Address National Aeronautics and Space Administration Washington, DC 20546		13. Type of Report and Period Covered Technical Memorandum
		14. Sponsoring Agency Code
15. Supplementary Notes		

16. Abstract

An investigation has been conducted in the Langley 7- by 10-foot tunnel to determine the influence of an optimized leading-edge deflection on the low-speed aerodynamic performance of a configuration with a low-aspect-ratio, highly swept wing. Tests have also been conducted to determine the sensitivity of the lateral-stability derivative (C_{l_β}) to geometric anhedral.

The optimized leading-edge deflection was developed by aligning the leading edge with the incoming flow along the entire span. Owing to the spanwise variation of upwash, the resulting optimized leading edge was a smooth, continuously warped surface for which the deflection varied from 16° at the side of body to 50° at the wing tip. For the particular configuration studied, levels of leading-edge suction on the order of 90 percent were achieved. The results of tests conducted to determine the sensitivity of C_{l_β} to geometric anhedral indicate values of $\partial C_{l_\beta}/\partial \Gamma$ which are in reasonable agreement with estimates provided by simple vortex-lattice theories.

17. Key Words (Suggested by Author(s)) Arrow wing; Swept wing; Leading-edge deflection	18. Distribution Statement Unclassified - Unlimited. Subject Category 02

19. Security Classif. (of this report)	20. Security Classif. (of this page)	21. No. of Pages	22. Price*
Unclassified	Unclassified	51	$5.25

* For sale by the National Technical Information Service, Springfield, Virginia 22161